

A reliability- and latency-driven task allocation framework for workflow applications in the edge-hub-cloud continuum

Andreas Kouloumpris^{a,b,*}, Georgios L. Stavrinides^b, Maria K. Michael^{a,b}, Theocharis Theocharides^{a,b}

^aDepartment of Electrical and Computer Engineering, University of Cyprus, 1 Panepistimiou Avenue, Aglantzia, P.O. Box 20537, Nicosia, 1678, Cyprus

^bKIOS Research and Innovation Center of Excellence, University of Cyprus, 1 Panepistimiou Avenue, Aglantzia, P.O. Box 20537, Nicosia, 1678, Cyprus

Abstract

A growing number of critical workflow applications leverage a streamlined edge-hub-cloud architecture, which diverges from the conventional edge computing paradigm. An edge device, in collaboration with a hub device and a cloud server, often suffices for their reliable and efficient execution. However, task allocation in this streamlined architecture is challenging due to device limitations and diverse operating conditions. Given the inherent criticality of such workflow applications, where reliability and latency are vital yet conflicting objectives, an exact task allocation approach is typically required to ensure optimal solutions. As no existing method holistically addresses these issues, we propose an exact multi-objective task allocation framework to jointly optimize the overall reliability and latency of a workflow application in the specific edge-hub-cloud architecture. We present a comprehensive binary integer linear programming formulation that considers the relative importance of each objective. It incorporates time redundancy techniques, while accounting for crucial constraints often overlooked in related studies. We evaluate our approach using a relevant real-world workflow application, as well as synthetic workflows varying in structure, size, and criticality. In the real-world application, our method achieved average improvements of 84.19% in reliability and 49.81% in latency over baseline strategies, across relevant objective trade-offs. Overall, the experimental results demonstrate the effectiveness and scalability of our approach across diverse workflow applications for the considered system architecture, highlighting its practicality with runtimes averaging between 0.03 and 50.94 seconds across all examined workflows.

Keywords: Task allocation, Reliability, Latency, Multi-objective optimization, Workflow applications, Edge-hub-cloud

1. Introduction

The technological advancements in edge computing and the Internet of Things (IoT) are spearheading the emergence of critical applications that require real-time response and reliable execution near the network edge [1]. Such applications typically comprise several component tasks with precedence relationships and are commonly referred to as *workflows* [2]. A prominent example is the use of an unmanned aerial vehicle (UAV) equipped with sensing and computational capabilities for the autonomous inspection of critical infrastructures (e.g., power transmission towers and lines) or for search-and-rescue missions in areas that are difficult to access from the ground [3, 4]. Another example is the use of implantable biomedical edge devices for remote patient monitoring and support, such as smart pacemakers [5–8]. These use-cases [3–8] commonly involve pre-programmed operations and leverage a streamlined architecture based on the *edge-hub-cloud* paradigm, where the edge device (e.g., UAV or smart pacemaker) interacts with a hub device (e.g., a laptop or smartphone), which in turn communicates with a cloud server to process certain tasks in a more reliable and timely manner. In such safety-critical scenarios, reliability

and latency are of paramount importance. Consequently, their joint optimization for workflow task allocation in the edge-hub-cloud continuum, subject to device- and application-specific constraints, is essential.

The edge-hub-cloud paradigm deviates from the conventional edge computing model, which typically comprises edge devices in the bottom layer, edge servers in the middle layer, and cloud servers in the top layer. In contrast, an edge-hub-cloud architecture employs edge and hub devices that may be battery-operated in the bottom layer, and cloud servers in the top layer. While a hub device may not be as powerful as an edge server, it is strategically positioned closer to the edge devices, facilitating their coordination and communication with the remote cloud servers more effectively. This streamlined architecture has become increasingly prevalent in real-world domains such as UAV-enabled infrastructure inspection and biomedical monitoring [3–8], where a single edge device, a hub device, and a cloud server often suffice for reliable and real-time execution.

However, the reliability, processing power, memory, storage, and energy capacity of the devices, as well as the capacity of the communication channels, typically decline when moving from the cloud towards the edge of the network [9]. These issues are further amplified by the diverse characteristics of the operating environment [10]. Specifically, the reliability of a device is not only dependent on technological factors, such as integrated circuit wear-out and aging, which may cause perma-

*Corresponding author.

Email address: kouloumpris.andreas@ucy.ac.cy (Andreas Kouloumpris)

nent errors, but it also depends on various environmental factors, such as temperature, humidity, electromagnetic interference, and cosmic rays, which may cause transient errors (e.g., soft errors). Moreover, the proliferation of hardware errors, either permanent or transient, is well known to be workload dependent [11]. Thus, an edge device, due to its lower manufacturing cost, higher integration, and the environmental conditions it operates in, is typically more vulnerable to reliability threats than a hub device, which in turn is often less reliable than a cloud server.

A widely used approach to increase the reliability of an application is time redundancy [12]. According to this method, a task is replicated and executed multiple times (two for error detection, three for error mitigation), and the outputs of all task executions are compared (dual execution) or subjected to a majority vote (triple execution). The number of executions for a specific task typically depends on the expected reliability of the task when executed on a particular device, as well as the criticality of the task or application. However, the additional overhead incurred by such techniques may impair the overall performance, especially in architectures with limited resources like the one considered in this work. Hence, maximizing the reliability and minimizing the latency of an application in the specific edge-hub-cloud environment are conflicting goals.

To achieve an optimized balance between reliability and latency based on the relative importance of each objective, task allocation plays a crucial role, as it determines which device should execute each task of the workflow. This is distinct from task scheduling, which focuses on the execution order and timing of tasks on a given device. In its general form, the task allocation problem is NP-hard [13]. The inherent criticality of the targeted applications necessitates the optimal mapping of tasks to system devices. This can be attained by utilizing an exact optimization method, namely binary integer linear programming (BILP), which yields a true Pareto-optimal solution for a given combination of objective weights [14]. In contrast to heuristics, which typically provide only approximate or near-Pareto-optimal solutions and thus may fail to satisfy all constraints, BILP can optimally capture the interplay between multiple constraints and objectives, enabling meaningful design-time trade-off exploration. Given the pre-programmed nature of the considered applications, BILP can be executed offline to accommodate its computational demands, provided that a solution can be obtained within a reasonable time.

Although the applications that motivate this work utilize a streamlined edge-hub-cloud architecture, the allocation of their tasks entails all the aforementioned challenges that must be addressed. To this end, we propose an exact, design-time (i.e., offline) multi-objective BILP-based optimization framework to allocate the tasks of a workflow application on an edge device, a hub device, and a cloud server. Our approach jointly optimizes the overall reliability and latency of the application, based on the desired trade-off between the two objectives. It takes into account the criticality of the application and multiple constraints, including the computational and energy limitations of the devices, the varied bandwidth of the communication links, and inter-device connectivity. The main contribu-

tions of this work, which builds upon our preliminary research in [15, 16], are summarized as follows:

1. We present a comprehensive formulation for modeling the considered problem as a multi-objective BILP model. The formulation is facilitated by a two-step task graph transformation technique, which encapsulates the application and system models, as well as the adopted energy and reliability models, while integrating time redundancy methods such as dual and triple task execution.
2. Our formulation jointly optimizes reliability and latency while holistically considering constraints often ignored in related research efforts, such as the limited memory, storage, and energy capacities of the devices, the reliability requirements of the tasks, as well as the computational and communication latency and energy required to execute each task.
3. We evaluate our approach using a real-world workflow application for the autonomous UAV-based aerial inspection of power transmission towers and lines.
4. To further validate and investigate the scalability and applicability of our method to workflows of different structures, sizes, and criticality levels, we use a suite of diverse synthetic workflows that we generated for this purpose.

To our knowledge, no existing method considers the same architecture, addresses the same objectives and constraints, and employs an exact multi-objective task allocation technique as our approach. The rest of the paper is organized as follows. Section 2 provides an overview of related literature. Section 3 describes the proposed optimization framework. Section 4 presents the experimental setup and the evaluation results, whereas Section 5 concludes the paper.

2. Related work

2.1. State-of-the-art task allocation methods for workflow applications

Several studies address the allocation of workflow tasks in distributed environments, with objectives targeting reliability [17], latency [18–22], or the joint optimization of both [23–36]. While some of these works also involve scheduling, our discussion is focused on task allocation.

2.1.1. Works optimizing either reliability or latency

Fang et al. [17] propose a multi-objective evolutionary algorithm for task allocation in multi-cloud systems that addresses cost, energy, and reliability, but not latency. Moreover, memory, storage, and communication energy constraints are not considered. In contrast, other works target latency as the optimization objective [18–22]. Jiang et al. [18], Nastic et al. [19], and Li et al. [20] investigate task allocation in heterogeneous multi-tier systems, but do not incorporate reliability into their objectives and constraints, while [19] and [20] also overlook the energy aspects of the problem. On the other hand, Santos et al. [21] and Marchese and Tomarchio [22] address container-based orchestration where reliability is included in the constraints, but

the energy and storage requirements of the tasks are not taken into account. Although these studies [17–22] investigate multi-tier environments, none of them examine the edge-hub-cloud architecture considered in this work. Among them, only Santos et al. [21] employ an exact approach, formulating the problem as a mixed integer linear programming model.

2.1.2. Works jointly optimizing reliability and latency

A large body of research has focused on the joint optimization of reliability and latency. Specifically, Wang et al. [23], Tang [24], and Khurana et al. [25] propose task placement heuristics for computational resources of varying reliability. Asghari-Alaie et al. [26] present a hybrid task allocation approach that leverages heuristics to explore the solution space, based on failure rates derived from system logs. Wang et al. [27] propose a heuristic method based on iterative task duplication. Although these works [23–27] generally address both computational and communication latency, they overlook the memory, storage, and energy requirements of the tasks.

On the other hand, Huang et al. [28] propose a reliability- and latency-aware task allocation heuristic that also considers the energy consumption of the system. Similarly, Taghinezhad-Niar and Taheri [29, 30] present a task placement framework that utilizes task duplication and schedule gaps to improve reliability and latency while reducing the energy consumption of computational resources. In the same context, Saeedi et al. [31] develop an enhanced many-objective particle swarm optimization approach, incorporating greedy heuristics for initial solution generation. Peng et al. [32] introduce heuristics based on the reliability-to-performance ratio of the application, under energy consumption constraints. However, none of these works [28–32] consider the energy required for inter-task communication, nor the memory and storage required by each task.

Efforts that specifically target multi-tier environments include [33] and [34]. In [33], De Maio et al. propose a genetic algorithm-based task allocation metaheuristic, aimed at finding the best trade-off between latency and reliability, while considering the storage requirements of the tasks. Similarly, a critical path-based task placement heuristic that takes into account the memory needs of the tasks is presented by Khaleel in [34]. Although both of these studies investigate multi-tier systems, they do not consider the specific architecture examined in this work, nor the energy demands of the application. While none of the multi-objective research efforts [23–34] utilize an exact method for solving the specific problem, an exact integer non-linear programming approach is employed by Ramezani et al. in [35]. The proposed method involves the segmentation of the application task graph and the optimization of each segment separately to achieve a balance between reliability and latency. Although an exact method is employed, the inter-task communication latency, a multi-tier environment, and the storage and energy requirements of the application are not taken into account. The study by Fan et al. [36], which is most closely related to our work, investigates the joint optimization of reliability and latency in a multi-tier system. However, similar to the majority of prior works, their approach neither incorporates

energy constraints nor considers the specific edge-hub-cloud architecture, and it does not utilize an exact optimization method.

2.1.3. Summary of research gaps

Overall, the presented state-of-the-art task allocation strategies for workflow applications [17–36] do not comprehensively address the joint optimization of reliability and latency under all the constraints considered in our work (i.e., memory, storage, computational and communication latency and energy, and reliability constraints), nor do they examine the specific edge-hub-cloud architecture. Moreover, in contrast to our approach, the vast majority of these efforts do not use an exact method to solve the task allocation problem. With respect to these aspects, Table 1 summarizes the qualitative comparison of our work with the state of the art.

2.2. Comparison with our preliminary research

In our preliminary studies [15, 16], we explored task allocation in an edge-hub-cloud environment, applying time redundancy techniques to gain initial insights into the resulting overall latency [15] and reliability [16], respectively. However, these initial studies were limited to single objectives and lacked a comprehensive optimization approach, motivating the current multi-objective problem. In another prior study [37], we considered either latency or energy optimization without incorporating reliability, using a simplified single-step task graph extension to facilitate the problem formulation. Moreover, although in [38] we investigated both task allocation and scheduling in an edge-hub-cloud architecture, we solely focused on latency optimization without considering reliability. In contrast, this work advances beyond these preliminary studies by formulating a holistic multi-objective task allocation framework that jointly optimizes reliability and latency. Additionally, we propose an enhanced two-step task graph transformation technique incorporating advanced models for both energy and reliability, thereby providing a novel and comprehensive solution to the problem under consideration.

3. Proposed multi-objective optimization framework

3.1. Framework overview

We formulate the examined task allocation problem as a multi-objective BILP model. BILP is an exact method suitable for modeling and solving problems of this nature and size at design-time [14]. Our formulation is facilitated by a two-step task graph transformation approach. In the first step, we transform the initial task graph (TG) of the workflow application into an intermediate edge-hub-cloud graph (EG). EG represents the possible allocations of the tasks on the considered devices, encapsulating both the application and system models. It also facilitates the definition of the energy and reliability models. In the second step, we transform EG into the final reliability-aware edge-hub-cloud graph (REG), taking into account the reliability requirements of each task, by integrating dual and triple task execution techniques. Finally, we use the resulting REG to formulate the considered problem. The problem is solved according

Table 1: Qualitative comparison with related state-of-the-art works on task allocation for workflow applications.

Ref.	Objectives		Constraints							Multi-Tier Environ.	Exact Method
	Reliability	Latency	Memory	Storage	Comp. Latency	Comp. Energy	Comm. Latency	Comm. Energy			
[17]	✓	-	-	-	✓	✓	✓	-	✓	✓	-
[18]	-	✓	-	-	✓	✓	✓	✓	-	✓	-
[19]	-	✓	✓	-	✓	-	✓	-	-	✓	-
[20]	-	✓	✓	-	✓	-	✓	-	-	✓	-
[21]	-	✓	✓	-	✓	-	✓	-	✓	✓	✓
[22]	-	✓	✓	-	✓	-	✓	-	✓	✓	-
[23]	✓	✓	-	-	✓	-	-	-	✓	-	-
[24]	✓	✓	-	-	✓	-	✓	-	✓	-	-
[25]	✓	✓	-	-	✓	-	✓	-	✓	-	-
[26]	✓	✓	-	-	✓	-	✓	-	✓	-	-
[27]	✓	✓	-	-	✓	-	✓	-	✓	-	-
[28]	✓	✓	-	-	✓	✓	✓	-	✓	-	-
[29]	✓	✓	-	-	✓	✓	✓	-	✓	-	-
[30]	✓	✓	-	-	✓	✓	✓	-	✓	✓	-
[31]	✓	✓	-	-	✓	✓	✓	-	✓	-	-
[32]	✓	✓	-	-	✓	✓	✓	-	✓	-	-
[33]	✓	✓	-	✓	✓	-	✓	-	✓	✓	-
[34]	✓	✓	✓	-	✓	-	✓	-	✓	✓	-
[35]	✓	✓	✓	-	✓	-	-	-	✓	-	✓
[36]	✓	✓	✓	✓	✓	-	✓	-	✓	✓	-
Ours	✓	✓	✓	✓	✓	✓	✓	✓	✓	✓	✓

to the defined trade-off between the two competing objectives, reliability and latency. Intuitively, the transformation from TG to EG and subsequently to REG makes all feasible task allocations and reliability-aware execution configurations explicit, enabling the BILP solver to select exactly one candidate allocation and time redundancy technique (when applicable) per task, while jointly optimizing reliability and latency.

3.2. Modeling assumptions

The proposed framework targets pre-programmed safety-critical workflow applications executed in a streamlined edge-hub-cloud architecture, where the workflow structure is static and known a priori. In line with the majority of related works in the field [17, 18, 24–27, 32–34, 36], we adopt an offline (design-time) optimization approach where the application, system, and network parameters are obtained through profiling or real-world measurements and treated as fixed inputs. This static approach is typical and appropriate in the targeted applications [3–8], where deterministic guarantees on reliability and latency are required. In contrast, dynamic exact methods are computationally infeasible, while heuristic online methods cannot guarantee optimal solutions, nor provide the same level of predictability.

3.3. Step 1 of TG transformation – intermediate EG

The TG of a workflow application that comprises a set of tasks $\mathcal{T} = \{1, 2, \dots, |\mathcal{T}|\}$, is typically represented by a directed acyclic graph $G = (\mathcal{N}, \mathcal{A})$ [39]. $\mathcal{N} = \{N_1, N_2, \dots, N_{|\mathcal{T}|}\}$ is the set of its nodes, whereas $\mathcal{A} = \{A_{i \rightarrow j} | N_i, N_j \in \mathcal{N}, N_i \neq N_j, N_i \rightarrow N_j\}$ is the set of its arcs. A node $N_i \in \mathcal{N}$ corresponds to a task $i \in \mathcal{T}$ of the application. An arc $A_{i \rightarrow j} \in \mathcal{A}$ between a node N_i (corresponding to a parent task i) and a node N_j (corresponding to a child task j), denotes the communication and precedence relationship between the two tasks.

In the first step of the task graph transformation, the initial TG G is transformed into the intermediate EG $\hat{G} = (\hat{\mathcal{N}}, \hat{\mathcal{A}})$,

based on the main principles of our approach in [37]. Specifically, each node $N_i \in \mathcal{N}$ in G is transformed into a composite node (i.e., a set of nodes) $\hat{N}_i \in \hat{\mathcal{N}}$ in \hat{G} , such that:

$$\hat{\phi}_{\text{node}}(N_i) = \hat{N}_i = \{N_{ik} | k \in Q_i \subseteq \mathcal{U}\}, \quad (1)$$

where $\hat{\phi}_{\text{node}}$ is the function that transforms the node N_i into the set \hat{N}_i as shown above, and \mathcal{U} is the set of devices in the examined edge-hub-cloud environment. k is a device in the subset of devices $Q_i \subseteq \mathcal{U}$ where task i can be allocated. If task i can be allocated on any device in \mathcal{U} , then $Q_i = \mathcal{U}$, otherwise $Q_i \subset \mathcal{U}$. Hence, an individual node $N_{ik} \in \hat{G}$ denotes the possible allocation of task i on device k .

Each arc $A_{i \rightarrow j} \in \mathcal{A}$ in G is transformed into a composite arc (i.e., a set of arcs) $\hat{A}_{i \rightarrow j} \in \hat{\mathcal{A}}$ in \hat{G} , such that:

$$\hat{\phi}_{\text{arc}}(A_{i \rightarrow j}) = \hat{A}_{i \rightarrow j} = \{A_{ik \rightarrow jl} = N_{ik} \rightarrow N_{jl} | k \in Q_i \subseteq \mathcal{U}, l \in Q_j \subseteq \mathcal{U}\}, \quad (2)$$

where $\hat{\phi}_{\text{arc}}$ is the function that transforms the arc $A_{i \rightarrow j}$ into the set $\hat{A}_{i \rightarrow j}$ as shown above. An individual arc $A_{ik \rightarrow jl} \in \hat{G}$ represents the communication and precedence relationship between the nodes it connects, N_{ik} and N_{jl} . It is noted that if the communication between devices k and l cannot be performed directly (e.g., between an edge device and a cloud server in the examined architecture), it is performed through an intermediate device (e.g., a hub device), incurring additional communication latency and energy costs. If both tasks i and j are on the same device (i.e., $k = l$), the involved communication cost is considered negligible compared to the case where $k \neq l$.

3.3.1. EG node parameters

A node $N_{ik} \in \hat{G}$ has the following parameters:

- M_i : main memory required by task i .
- S_i : storage required by task i .
- D_i : size of output data generated by task i .

- L_{ik} : execution time of task i on device k .
- P_{ik} : power required to execute task i on device k .
- E_{ik} : energy required to execute task i on device k .
- V_{ik} : vulnerability factor of task i on device k (i.e., probability that the execution of task i on device k fails).
- R_{ik} : reliability of task i on device k (i.e., probability that task i is executed on device k without any failures).
- ϵ_{ik} : execution mode of task i when allocated on device k , indicating whether task i requires single execution (SE) on device k , or dual execution (DE) or triple execution (TE), where the replicated executions may be performed on the same or on different devices to increase reliability.
- v_i : number of child tasks of task i (i.e., number of immediate successor nodes of node $N_i \in G$).

Parameters M_i , S_i , D_i , and v_i are device-independent, whereas L_{ik} , P_{ik} , E_{ik} , V_{ik} , R_{ik} , and ϵ_{ik} are device-dependent. M_i , S_i , D_i , L_{ik} , and P_{ik} can be defined through performance profiling and power monitoring tools, as explained in Section 4. E_{ik} is given by (5), based on the energy model described in Section 3.4. V_{ik} can be profiled via well-known approaches based on fault injection techniques and/or architecturally correct execution (ACE) analysis [40, 41]. R_{ik} and ϵ_{ik} are defined by (9) and (10), respectively, based on the reliability model presented in Section 3.5. Finally, v_i is a structural characteristic of G and thus easily derived.

3.3.2. EG arc parameters

An arc $A_{ik \rightarrow jl} \in \dot{G}$ has the following parameters:

- $\zeta_{ik \rightarrow jl}^o$: binary parameter indicating whether $A_{ik \rightarrow jl}$ involves indirect communication between devices k and l , through intermediate device o :

$$\zeta_{ik \rightarrow jl}^o = \begin{cases} 1, & \text{if devices } k \text{ and } l \text{ cannot communicate} \\ & \text{directly and communication is} \\ & \text{performed via device } o, \\ 0, & \text{otherwise.} \end{cases} \quad (3)$$

- $CL_{ik \rightarrow jl}$: time required to transfer the output data D_i of task i (on device k) to task j (on device l):

$$CL_{ik \rightarrow jl} = \begin{cases} D_i / \sigma_{kl}, & \text{if } \zeta_{ik \rightarrow jl}^o = 0, \\ & k \neq l, \\ D_i (1 / \sigma_{ko} + 1 / \sigma_{ol}), & \text{if } \zeta_{ik \rightarrow jl}^o = 1, \\ 0, & \text{if } k = l, \end{cases} \quad (4)$$

where σ_{kl} , σ_{ko} , and σ_{ol} denote the bandwidth of the communication channels between the respective devices.

- $CE_{ik \rightarrow jl}$: energy required to transfer the output data D_i of task i (on device k) to task j (on device l). It is given by (6), based on the energy model in Section 3.4.

3.3.3. Transformation examples (EG)

Fig. 1 illustrates two examples of our two-step transformation technique. The initial TG G of an application with two tasks is shown in Fig. 1a. The considered edge-hub-cloud architecture comprises a single edge device (e), a single hub device (h), and a single cloud server (c), i.e., $\mathcal{U} = \{e, h, c\}$. In step 1 of the first example (Fig. 1b), G is transformed into \dot{G} considering that both tasks can be allocated on any device, i.e., $Q_1 = Q_2 = \mathcal{U} = \{e, h, c\}$. In step 1 of the second example (Fig. 1c), G is transformed into \dot{G} considering that task 1 requires fixed allocation on device e ($Q_1 = \{e\}$), and task 2 on device h or c ($Q_2 = \{h, c\}$). In both examples, we assume that a task requires triple (TE), dual (DE), or single (SE) execution if it is allocated on device e, h, or c, respectively. The arcs involving devices e and c, which cannot communicate directly, are depicted in orange. Step 2 of each example is described in Section 3.6.3.

3.4. Energy model

The computational energy E_{ik} required to execute task i on device k is given by [30, 31]:

$$E_{ik} = L_{ik} P_{ik}. \quad (5)$$

The communication energy $CE_{ik \rightarrow jl}$ required to transfer the output data D_i of task i , allocated on device k , to task j , allocated on device l , is defined as [6]:

$$CE_{ik \rightarrow jl} = \begin{cases} D_i (\tau_{kl} + \rho_{kl}), & \text{if } \zeta_{ik \rightarrow jl}^o = 0, \\ & k \neq l, \\ D_i (\tau_{ko} + \rho_{ko} + \tau_{ol} + \rho_{ol}), & \text{if } \zeta_{ik \rightarrow jl}^o = 1, \\ 0, & \text{if } k = l, \end{cases} \quad (6)$$

where τ_{kl} , τ_{ko} , and τ_{ol} (ρ_{kl} , ρ_{ko} , and ρ_{ol}) denote the energy required to transmit (receive) a unit of data over the respective communication channels. This energy model builds upon established formulations widely adopted in related studies [6, 30, 31]. It captures both the computational and communication energy required for workflow execution in the examined edge-hub-cloud architecture, while remaining independent of low-level architectural details for broader applicability.

3.5. Reliability model

We consider a criticality level $\Lambda \in \{1, 2, \dots, \Lambda_{\max}\}$ for the examined application. A higher Λ denotes a higher criticality and thus a lower vulnerability tolerance (Λ_{\max} is the highest criticality level). We employ two thresholds to represent the vulnerability tolerance of the application: (a) a vulnerability threshold for *dual task execution*, which is inversely proportional to Λ :

$$VT_{DE} = \frac{\kappa}{\Lambda}, \quad (7)$$

and (b) a vulnerability threshold for *triple task execution*:

$$VT_{TE} = \lambda VT_{DE}, \lambda > 1, \quad (8)$$

where κ and λ are adjustment coefficients. VT_{DE} and VT_{TE} are used in (10) to determine if a task i of the application, when

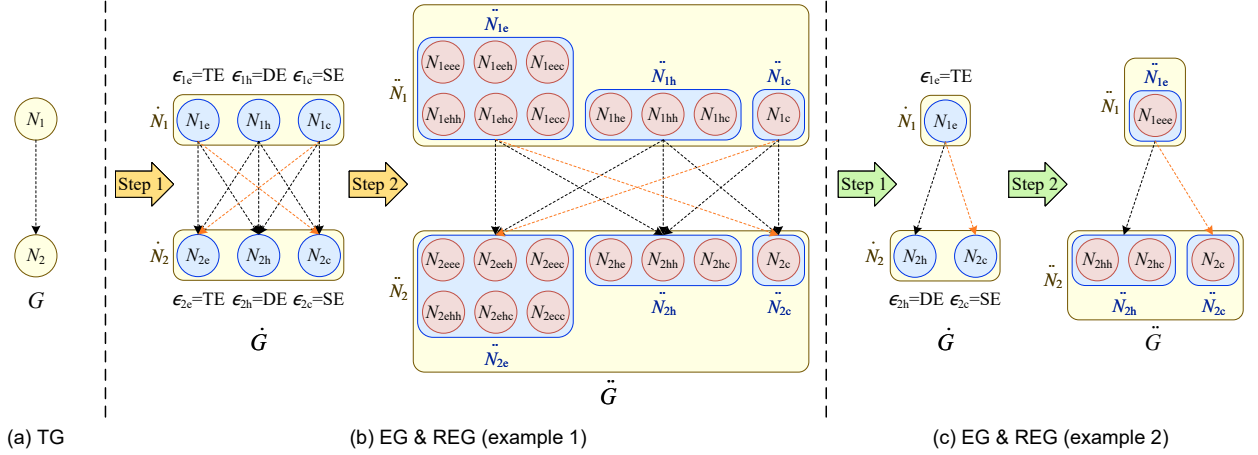


Figure 1: Examples of transforming an application's initial TG G into its corresponding intermediate EG \tilde{G} and final REG \ddot{G} .

allocated on a device k , requires (based on its vulnerability factor V_{ik}) duplication or triplication, respectively, to increase its reliability [12]. As V_{ik} is the probability the execution of task i on device k fails, we consider that $0 < V_{ik} < 1$. Hence, the reliability of task i on device k is given by [29, 42]:

$$R_{ik} = 1 - V_{ik}. \quad (9)$$

The execution mode ϵ_{ik} of task i when allocated on device k depends on V_{ik} , VT_{DE} , and VT_{TE} , as follows:

$$\epsilon_{ik} = \begin{cases} \text{SE}, & \text{if } V_{ik} < VT_{DE}, \\ \text{DE}, & \text{if } VT_{DE} \leq V_{ik} < VT_{TE}, \\ \text{TE}, & \text{if } VT_{TE} \leq V_{ik}. \end{cases} \quad (10)$$

If $\epsilon_{ik} = \text{SE}$, task i is executed only once on device k , as its reliability requirements are met. Otherwise, if $\epsilon_{ik} = \text{DE}$ or $\epsilon_{ik} = \text{TE}$, task i is replicated and executed twice or three times, respectively, either sequentially on the same device or in parallel on different devices, to increase its reliability. If $\epsilon_{ik} = \text{DE}$, the outputs of both executions of task i are compared (for error detection), whereas if $\epsilon_{ik} = \text{TE}$, the outputs of all three executions are subjected to a majority vote (for error mitigation). It is noted that in this work we consider transient errors. We use ϵ_{ik} to transform \dot{G} into \tilde{G} , as described in Section 3.6. The adopted reliability model is based on widely used dual and triple execution techniques for detecting and mitigating transient errors [12, 29, 42]. By linking application criticality to vulnerability thresholds, it enforces stricter reliability requirements at higher criticality levels, effectively capturing the dependencies between reliability and task allocation in the examined edge-hub-cloud architecture.

3.6. Step 2 of TG transformation – final REG

In the second step of the task graph transformation, the intermediate EG \tilde{G} is transformed into the final REG $\ddot{G} = (\ddot{N}, \ddot{A})$, by considering for each node $N_{ik} \in \tilde{G}$ the task replication technique determined by (10). Specifically, each composite node

$\dot{N}_i \in \dot{N}$ in \dot{G} is transformed into another composite node $\ddot{N}_i \in \ddot{N}$ in \ddot{G} , such that:

$$\ddot{\phi}_{\text{node}}(\dot{N}_i) = \ddot{N}_i = \{\ddot{N}_{ik} \mid \dot{N}_{ik} = \dot{\psi}(N_{ik}), N_{ik} \in \dot{N}_i\}, \quad (11)$$

where $\ddot{\phi}_{\text{node}}$ is the function that transforms the set \dot{N}_i into the final set \ddot{N}_i as shown above. $\dot{\psi}$ is the function that transforms each individual node $N_{ik} \in \dot{N}_i$ into the set $\ddot{N}_{ik} \in \ddot{N}_i$, so that:

$$\ddot{N}_{ik} = \begin{cases} \{N_{ik} = \{r_{ik}^1\}\}, & \text{if } \epsilon_{ik} = \text{SE}, \\ \{N_{ikl} = \{r_{ik}^1, r_{il}^2\} \mid l \in \mathcal{Q}_i\}, & \text{if } \epsilon_{ik} = \text{DE}, \\ \{N_{iklm} = \{r_{ik}^1, r_{il}^2, r_{im}^3\} \mid l, m \in \mathcal{Q}_i\}, & \text{if } \epsilon_{ik} = \text{TE}, \end{cases} \quad (12)$$

where r_{in}^z represents the allocation of primary task i or one of its replicas on device n . Specifically, if $z = 1$, it denotes *primary* task i , allocated on its initially assigned (as in \dot{G}) device k (*primary device*). If $z = 2$ or $z = 3$, it denotes a *replica* of task i , allocated on device $l \in \mathcal{Q}_i$ or $m \in \mathcal{Q}_i$, respectively (l and/or m may be the same as the primary device k).

Consequently, if $\epsilon_{ik} = \text{SE}$, $N_{ik} \in \tilde{G}$ remains as one node $N_{ik} \in \ddot{G}$, representing the allocation of primary task i on primary device k . On the other hand, if $\epsilon_{ik} = \text{DE}$, $N_{ik} \in \tilde{G}$ is transformed into a set of nodes $\ddot{N}_{ik} \in \ddot{G}$. Each individual node $N_{ikl} \in \ddot{N}_{ik}$ represents the duplication of task i , so that primary task r_{ik}^1 is allocated on primary device k and its replica r_{il}^2 is allocated on device l . If $l \neq k$, r_{il}^2 sends its output back to device k . The outputs of r_{ik}^1 and r_{il}^2 are compared on device k (for error detection). Similarly, if $\epsilon_{ik} = \text{TE}$, $N_{ik} \in \tilde{G}$ is transformed into a set of nodes $\ddot{N}_{ik} \in \ddot{G}$. Each individual node $N_{iklm} \in \ddot{N}_{ik}$ represents the triplication of task i , so that r_{ik}^1 is allocated on device k , whereas r_{il}^2 and r_{im}^3 are allocated on devices l and m , respectively. If $l \neq k$ and/or $m \neq k$, r_{il}^2 and/or r_{im}^3 , respectively, send their outputs back to device k . A majority vote is taken on device k on the outputs of r_{ik}^1 , r_{il}^2 , and r_{im}^3 (for error mitigation).

For notational convenience, an individual node N_{ik} , N_{ikl} , or N_{iklm} in \ddot{G} ($k, l, m \in \mathcal{Q}_i$) is denoted in abstracted form as $N_{\dot{ik}}$, and is referred to as *candidate node*. The possible cases of the non-abstracted form of $N_{\dot{ik}}$, with respect to the devices where

its task replicas may be allocated, are defined as:

$$N_{i\hat{k}} = N_{ik}, \quad \text{if } \epsilon_{ik} = \text{SE}, \quad (13)$$

$$= N_{ikk}, \quad \text{if } \epsilon_{ik} = \text{DE}, k = l, \quad (14)$$

$$= N_{ikl}, \quad \text{if } \epsilon_{ik} = \text{DE}, k \neq l, \quad (15)$$

$$= N_{ikkk}, \quad \text{if } \epsilon_{ik} = \text{TE}, k = l = m, \quad (16)$$

$$= N_{ikkm}, \quad \text{if } \epsilon_{ik} = \text{TE}, k = l \neq m, \quad (17)$$

$$= N_{ikll}, \quad \text{if } \epsilon_{ik} = \text{TE}, k \neq l = m, \quad (18)$$

$$= N_{iklm}, \quad \text{if } \epsilon_{ik} = \text{TE}, k \neq l \neq m. \quad (19)$$

These cases are referenced in (21)–(23) to maintain brevity.

For an arc $A_{ik \rightarrow jl} \in \dot{G}$, the communication between any two candidate nodes $N_{i\hat{k}} \in \dot{N}_{ik}$ and $N_{j\hat{l}} \in \dot{N}_{jl}$ in \dot{G} is performed over the communication channel between primary devices k and l , regardless of where the task replicas in $N_{i\hat{k}}$ and $N_{j\hat{l}}$ are allocated. Therefore, each composite arc $\dot{A}_{i \rightarrow j} \in \dot{\mathcal{A}}$ in \dot{G} is transformed into another composite arc $\dot{A}_{i \rightarrow j} \in \dot{\mathcal{A}}$ in \dot{G} , such that:

$$\begin{aligned} \dot{\phi}_{\text{arc}}(\dot{A}_{i \rightarrow j}) = \dot{A}_{i \rightarrow j} = \{ & A_{ik \rightarrow jl} = \dot{N}_{ik} \rightarrow \dot{N}_{jl} \\ & | A_{ik \rightarrow jl} \in \dot{A}_{i \rightarrow j} \}, \end{aligned} \quad (20)$$

where $\dot{\phi}_{\text{arc}}$ is the function that transforms the set $\dot{A}_{i \rightarrow j}$ into the final set $\dot{A}_{i \rightarrow j}$ as shown above. Hence, an individual arc $A_{ik \rightarrow jl}$ between nodes N_{ik} and N_{jl} in \dot{G} is retained as arc $A_{ik \rightarrow jl}$ between corresponding sets \dot{N}_{ik} and \dot{N}_{jl} in \dot{G} .

3.6.1. REG candidate node parameters

A candidate node $N_{i\hat{k}} \in \dot{G}$ inherits ϵ_{ik} and v_i from $N_{ik} \in \dot{G}$. Each primary task or replica $r_{in}^z \in N_{i\hat{k}}$ inherits M_i , S_i , D_i , L_{in} , P_{in} , E_{in} , V_{in} , and R_{in} from the respective node $N_{in} \in \dot{G}$. Additionally, $N_{i\hat{k}}$ has the following aggregate parameters:

- $L_{i\hat{k}}$: total time required to execute primary task i and its replicas on their allocated devices, including the time required to transfer the input data D_j from primary device k to the devices of the replicas, return the output D_i of each replica back to device k , and perform the comparison/voting on device k . It is defined based on the different forms of $N_{i\hat{k}}$ in (13)–(19):

$$L_{i\hat{k}} = \begin{cases} L_{ik}, & \text{if (13),} \\ 2L_{ik} + \beta_k^{\text{DE}}, & \text{if (14),} \\ \max\{L_{ik}, \frac{D_j}{\sigma_{kl}} + L_{il} + \frac{D_i}{\sigma_{ik}}\} + \beta_k^{\text{DE}}, & \text{if (15),} \\ 3L_{ik} + \beta_k^{\text{TE}}, & \text{if (16),} \\ \max\{2L_{ik}, \frac{D_j}{\sigma_{km}} + L_{im} + \frac{D_i}{\sigma_{mk}}\} + \beta_k^{\text{TE}}, & \text{if (17),} \\ \max\{L_{ik}, \frac{D_j}{\sigma_{kl}} + 2(L_{il} + \frac{D_i}{\sigma_{ik}})\} + \beta_k^{\text{TE}}, & \text{if (18),} \\ \max\{L_{ik}, \frac{D_j}{\sigma_{kl}} + L_{il} + \frac{D_i}{\sigma_{ik}}, \\ \frac{D_j}{\sigma_{km}} + L_{im} + \frac{D_i}{\sigma_{mk}}\} + \beta_k^{\text{TE}}, & \text{if (19),} \end{cases} \quad (21)$$

where β_k^{DE} and β_k^{TE} denote the time required to perform the comparison and voting, respectively, on device k .

- $E_{in}^{z,i\hat{k}}$: total energy required by device n to execute r_{in}^z , including (a) the energy required to receive r_{in}^z 's input D_j from primary device k and transmit back its output D_i (if

$n \neq k$), or (b) the energy required to transmit D_j to the devices of the replicas, receive D_i from each replica, and execute the comparison/voting (if $n = k$). It is defined based on the different forms of $N_{i\hat{k}}$ in (13)–(19), considering if r_{in}^z is the primary task ($z = 1$) or not ($z \in \{2, 3\}$), and if $n = k$ or $n \neq k$:

$$E_{in}^{z,i\hat{k}} = \begin{cases} E_{ik}, & \text{if } z = 1 \wedge (13) \\ \vee (z \in \{2, 3\} \wedge ((14) \vee (16) \vee ((17) \wedge n = k))), \\ E_{ik} + \delta_k^{\text{DE}}, & \text{if } z = 1 \wedge (14), \\ E_{ik} + D_j \tau_{kl} + D_i \rho_{lk} + \delta_k^{\text{DE}}, & \text{if } z = 1 \wedge (15), \\ E_{ik} + \delta_k^{\text{TE}}, & \text{if } z = 1 \wedge (16), \\ E_{ik} + D_j \tau_{km} + D_i \rho_{mk} + \delta_k^{\text{TE}}, & \text{if } z = 1 \wedge (17), \\ E_{ik} + D_j \tau_{kl} + 2D_i \rho_{lk} + \delta_k^{\text{TE}}, & \text{if } z = 1 \wedge (18), \\ E_{ik} + D_j (\tau_{kl} + \tau_{km}) \\ + D_i (\rho_{lk} + \rho_{mk}) + \delta_k^{\text{TE}}, & \text{if } z = 1 \wedge (19), \\ D_j \rho_{kl} + E_{il} + D_i \tau_{lk}, & \text{if } z \in \{2, 3\} \\ \wedge ((15) \vee (18) \vee ((19) \wedge n = l)), \\ D_j \rho_{km} + E_{im} + D_i \tau_{mk}, & \text{if } z \in \{2, 3\} \\ \wedge ((17) \vee (19)) \wedge n = m, \end{cases} \quad (22)$$

where $\delta_k^{\text{DE}} = \beta_k^{\text{DE}} \gamma_k^{\text{DE}}$ and $\delta_k^{\text{TE}} = \beta_k^{\text{TE}} \gamma_k^{\text{TE}}$ denote the energy required to perform the comparison and voting, respectively, on device k . γ_k^{DE} and γ_k^{TE} indicate the power consumption in each case.

- $V_{i\hat{k}}$: total vulnerability factor of $N_{i\hat{k}}$, i.e., probability that the execution of primary task i and all of its replicas fails. It depends on the different forms of $N_{i\hat{k}}$ in (13)–(19), as follows [29]:

$$V_{i\hat{k}} = \begin{cases} V_{ik}, & \text{if (13),} \\ (V_{ik})^2, & \text{if (14),} \\ V_{ik} V_{il}, & \text{if (15),} \\ (V_{ik})^3, & \text{if (16),} \\ (V_{ik})^2 V_{im}, & \text{if (17),} \\ V_{ik} (V_{il})^2, & \text{if (18),} \\ V_{ik} V_{il} V_{im}, & \text{if (19).} \end{cases} \quad (23)$$

- $R_{i\hat{k}}$: total reliability of $N_{i\hat{k}}$, i.e., probability that primary task i or at least one of its replicas is executed without any failures. It is given by [42]:

$$R_{i\hat{k}} = 1 - V_{i\hat{k}}. \quad (24)$$

Without loss of generality, in (21) and (22) we consider that each pair of devices communicate directly. If the communication is indirect, then the same conditions hold, but the relevant σ , τ , and ρ parameters are used.

3.6.2. REG arc parameters

An arc $A_{ik \rightarrow jl} \in \dot{G}$ has the same parameters $\zeta_{ik \rightarrow jl}^o$, $CL_{ik \rightarrow jl}$, and $CE_{ik \rightarrow jl}$ as $A_{ik \rightarrow jl} \in \dot{G}$.

3.6.3. Transformation examples (REG)

Each intermediate EG \hat{G} described in Section 3.3.3 is transformed into the corresponding REG \check{G} as illustrated by step 2 in Figs. 1b and 1c. Specifically, each node $N_{ik} \in \hat{G}$ is transformed into a set $\check{N}_{ik} \in \check{G}$, based on ϵ_{ik} . Each set $\check{N}_{ik} \in \check{G}$ comprises candidate nodes that represent the possible allocations of the primary task and its replicas in each case. For instance, in the first example (Fig. 1b), if task 1 is allocated on device e (denoted by $N_{1e} \in \hat{G}$), it requires triple execution. The possible allocations of its replicas on its eligible devices ($\mathcal{Q}_1 = \mathcal{U} = \{e, h, c\}$) are represented by the six candidate nodes in set $\check{N}_{1e} \in \check{G}$. On the other hand, in the second example (Fig. 1c), task 1 can only be allocated on device e. Since $N_{1e} \in \hat{G}$ requires triple execution, $\check{N}_{1e} \in \check{G}$ solely consists of candidate node N_{1eee} . As in \check{G} , the arcs involving devices e and c are shown in orange.

3.6.4. Impact of transformation on task graph size

Evidently, the transformation of the initial TG G into the final REG \check{G} increases the size of the resulting graph. In the worst case, where no task requires fixed allocation and all nodes in the intermediate EG \hat{G} require triple execution, for u different devices, the number of nodes in \check{G} increases by $u^2(u+1)/2$ times, whereas the number of arcs increases by u^2 times, with respect to those in G .

3.7. Multi-objective BILP formulation

We utilize the resulting REG \check{G} to formulate the problem as a BILP model, as follows:

3.7.1. Decision variables

We employ the following variables:

- A binary variable $x_{i\hat{k}}$ corresponding to a candidate node $N_{i\hat{k}} \in \check{G}$, such that $x_{i\hat{k}} = 1$ if $N_{i\hat{k}}$ is selected, and $x_{i\hat{k}} = 0$ otherwise.
- A binary variable $x_{ik \rightarrow jl}$ corresponding to an arc $A_{ik \rightarrow jl} \in \check{G}$, such that $x_{ik \rightarrow jl} = 1$ if $A_{ik \rightarrow jl}$ is selected, and $x_{ik \rightarrow jl} = 0$ otherwise.
- An auxiliary binary variable $x_{in}^{z,i\hat{k}}$ corresponding to a primary task or a replica $r_{in}^z \in N_{i\hat{k}}$, such that $x_{in}^{z,i\hat{k}} = 1$ if r_{in}^z is selected, and $x_{in}^{z,i\hat{k}} = 0$ otherwise.
- An auxiliary binary variable x_{ik} corresponding to a set $\check{N}_{ik} \in \check{G}$, such that $x_{ik} = 1$ if \check{N}_{ik} is selected, and $x_{ik} = 0$ otherwise.

3.7.2. Objective 1

The first objective aims to maximize the overall reliability of the application on the target system. The overall reliability denotes the probability that each primary task of the application, or at least one of its replicas, is executed on its allocated device without any failures. It is given by [29]:

$$R(\check{G}) = \prod_{N_{i\hat{k}} \in \check{N}} (R_{i\hat{k}})^{x_{i\hat{k}}}. \quad (25)$$

To formulate the objective function, we first linearize (25) by taking its logarithm [35, 43]:

$$\log(R(\check{G})) = \sum_{N_{i\hat{k}} \in \check{N}} \log(R_{i\hat{k}}) x_{i\hat{k}}. \quad (26)$$

Thus, we define the first objective function as:

$$f_{\text{rel}} = \sum_{N_{i\hat{k}} \in \check{N}} \log(R_{i\hat{k}}) x_{i\hat{k}}. \quad (27)$$

3.7.3. Objective 2

The second objective aims to minimize the overall latency of the application, which is defined by:

$$f_{\text{lat}} = \sum_{N_{i\hat{k}} \in \check{N}} L_{i\hat{k}} x_{i\hat{k}} + \sum_{A_{ik \rightarrow jl} \in \check{A}} CL_{ik \rightarrow jl} x_{ik \rightarrow jl}. \quad (28)$$

3.7.4. Multi-objective

As the two objectives, reliability and latency, have different scales, we first normalize (27) and (28) in the interval $[0, 1]$ [14]:

$$f'_{\text{rel}} = \frac{f_{\text{rel}} - \min(f_{\text{rel}})}{\max(f_{\text{rel}}) - \min(f_{\text{rel}})}, \quad (29)$$

and

$$f'_{\text{lat}} = \frac{f_{\text{lat}} - \min(f_{\text{lat}})}{\max(f_{\text{lat}}) - \min(f_{\text{lat}})}. \quad (30)$$

Since we can either minimize or maximize the combined objective, we convert the minimization of latency to a maximization problem, by considering the negation of (30):

$$f''_{\text{lat}} = -f'_{\text{lat}}. \quad (31)$$

Hence, we formulate the multi-objective function as:

$$g = w_{\text{rel}} f'_{\text{rel}} + w_{\text{lat}} f''_{\text{lat}}, \quad (32)$$

where w_{rel} and w_{lat} are predefined weights reflecting the relative importance of reliability and latency, respectively, in the combined objective. It is noted that $0 \leq w_{\text{rel}}, w_{\text{lat}} \leq 1$ and $w_{\text{rel}} + w_{\text{lat}} = 1$. Consequently, the considered multi-objective problem is defined as:

$$\max g \quad (33)$$

subject to the constraints defined in Section 3.7.5. We utilize the weighted sum approach, as the individual objective functions and the considered constraints are linear. In the context of BILP, which is an exact method, solving (33) for a given pair of objective weights yields a single Pareto-optimal solution [14]. Hence, the proposed framework does not aim to generate the entire set of Pareto-optimal solutions (Pareto front) in a single execution. In contrast, by varying the objective weights across different runs, different Pareto-optimal solutions can be explored, reflecting alternative trade-offs between reliability and latency. The weighted sum formulation is simple, practical, and easy to implement, while allowing direct control over the relative importance of the individual objectives.

3.7.5. Constraints

The multi-objective function (32) is maximized subject to the following constraints:

$$x_{i\hat{k}} \in \{0, 1\}, \forall N_{i\hat{k}} \in \check{\mathcal{N}}, \quad (34)$$

$$x_{ik \rightarrow jl} \in \{0, 1\}, \forall A_{ik \rightarrow jl} \in \check{\mathcal{A}}, \quad (35)$$

$$x_{in}^{\hat{z}, i\hat{k}} \in \{0, 1\}, \forall r_{in}^{\hat{z}} \in N_{i\hat{k}}, \forall N_{i\hat{k}} \in \check{\mathcal{N}}, \quad (36)$$

$$x_{ik} \in \{0, 1\}, \forall \check{N}_{ik} \in \check{\mathcal{N}}, \quad (37)$$

$$\sum_{N_{i\hat{k}} \in \check{\mathcal{N}}_i} x_{i\hat{k}} = 1, \forall \check{N}_i \in \check{\mathcal{N}}, \quad (38)$$

$$x_{ik} = \sum_{N_{i\hat{k}} \in \check{\mathcal{N}}_{ik}} x_{i\hat{k}}, \forall \check{N}_{ik} \in \check{\mathcal{N}}, \quad (39)$$

$$x_{i\hat{k}} |N_{i\hat{k}}| = \sum_{r_{in}^{\hat{z}} \in N_{i\hat{k}}} x_{in}^{\hat{z}, i\hat{k}}, \forall N_{i\hat{k}} \in \check{\mathcal{N}}, \quad (40)$$

$$\sum_{A_{ik \rightarrow jl} \in \check{\mathcal{A}}_i} x_{ik \rightarrow jl} = v_i, \forall \check{N}_i \in \check{\mathcal{N}}, \quad (41)$$

$$x_{ik \rightarrow jl} \leq x_{ik}, \forall A_{ik \rightarrow jl} \in \check{\mathcal{A}}, \quad (42)$$

$$x_{ik \rightarrow jl} \leq x_{jl}, \forall A_{ik \rightarrow jl} \in \check{\mathcal{A}}, \quad (43)$$

$$x_{ik \rightarrow jl} \geq x_{ik} + x_{jl} - 1, \forall A_{ik \rightarrow jl} \in \check{\mathcal{A}}, \quad (44)$$

$$\sum_{N_{i\hat{k}} \in \check{\mathcal{N}}} \sum_{r_{in}^{\hat{z}} \in N_{i\hat{k}}} M_i x_{in}^{\hat{z}, i\hat{k}} \leq M_n^{\text{bgt}}, \forall n \in \mathcal{U}, \quad (45)$$

$$\sum_{N_{i\hat{k}} \in \check{\mathcal{N}}} \sum_{r_{in}^{\hat{z}} \in N_{i\hat{k}}} S_i x_{in}^{\hat{z}, i\hat{k}} \leq S_n^{\text{bgt}}, \forall n \in \mathcal{U}, \quad (46)$$

$$\begin{aligned} & \sum_{N_{i\hat{k}} \in \check{\mathcal{N}}} \sum_{r_{in}^{\hat{z}} \in N_{i\hat{k}}} E_{in}^{\hat{z}, i\hat{k}} x_{in}^{\hat{z}, i\hat{k}} \\ & + \sum_{A_{in \rightarrow jl} \in \check{\mathcal{A}}} D_i x_{in \rightarrow jl} (\tau_{nl} (1 - \zeta_{in \rightarrow jl}^o) + \tau_{no} \zeta_{in \rightarrow jl}^o) \\ & + \sum_{A_{jl \rightarrow in} \in \check{\mathcal{A}}} D_j x_{jl \rightarrow in} (\rho_{ln} (1 - \zeta_{jl \rightarrow in}^o) + \rho_{on} \zeta_{jl \rightarrow in}^o) \\ & + \sum_{A_{il \rightarrow jo} \in \check{\mathcal{A}}} D_i x_{il \rightarrow jo} (\rho_{ln} + \tau_{no}) \zeta_{il \rightarrow jo}^n \\ & \leq E_n^{\text{bgt}}, \forall n \in \mathcal{U}, n \neq l \neq o. \end{aligned} \quad (47)$$

Equations (34)–(37) guarantee the binary nature of the decision variables. Constraint (38) ensures that only one candidate node $N_{i\hat{k}}$ in each set $\check{N}_i \in \check{\mathcal{N}}$ will be selected. That is, it ensures that only one of the possible allocations of each primary task i and its replicas (if applicable) will be selected. On the other hand, (39) ensures that if a candidate node $N_{i\hat{k}}$ is selected, the corresponding set \check{N}_{ik} in which $N_{i\hat{k}}$ belongs, will be selected as well. Equation (40) guarantees that if a candidate node $N_{i\hat{k}}$ is selected, its corresponding primary task and its replicas $r_{in}^{\hat{z}} \in N_{i\hat{k}}$ will also be selected.

Constraint (41) ensures that for each set $\check{N}_i \in \check{\mathcal{N}}$ (and by extension, for each selected candidate node $N_{i\hat{k}}$), the number of outgoing arcs that will be selected will be equal to the number of child tasks of task i . In the same context, (42)–(44) guarantee

that if two candidate nodes $N_{i\hat{k}} \in \check{N}_{ik}$ and $N_{j\hat{l}} \in \check{N}_{jl}$, respectively, are selected, the corresponding arc $A_{ik \rightarrow jl}$ will also be selected. Consequently, (41)–(44) ensure that the connectivity and precedence relationships between the candidate nodes in \check{G} – and thus between the nodes in the initial TG G – will be preserved.

Finally, (45)–(47) guarantee that the memory, storage, and energy budgets (M_n^{bgt} , S_n^{bgt} , and E_n^{bgt} , respectively) for each device $n \in \mathcal{U}$ will not be exceeded for the execution of the application. M_n^{bgt} , S_n^{bgt} , and E_n^{bgt} are typically defined based on the respective resources of each device. It is noted that the energy constraint in (47) includes both the computational and communication energy consumption of device $n \in \mathcal{U}$. Regarding the communication energy, we consider three cases: (a) device n transmits data to another device l (either directly or indirectly via device o), (b) n receives data from l (directly or indirectly through o), and (c) n is utilized for the communication between l and o . As the candidate nodes in \check{G} incorporate the reliability constraints of the tasks, our formulation ensures the exploration of only reliability-feasible allocations. The main notations used in our approach are listed in Table 2.

3.7.6. Complexity

The computational complexity of the proposed BILP framework depends on both the problem size and the employed solver. Well-established solvers such as Gurobi [44] typically use proprietary algorithms whose implementation details are not publicly available, and thus their computational complexity cannot be derived [11]. On the other hand, the problem size (i.e., the number of variables and constraints) depends on the size of the resulting REG \check{G} , whose growth relative to the initial TG G is analyzed in Section 3.6.4. Despite the size increase in \check{G} , our scalability analysis in Section 4.3.2 demonstrates that the proposed framework provides optimal solutions within practical time frames, even for TGs with 1000 tasks. Thus, the benefits of our approach significantly outweigh the additional complexity introduced by the size increase in \check{G} .

4. Framework evaluation

We evaluated our framework using a real-world workflow application for the autonomous UAV-based aerial inspection of power transmission towers and lines. Furthermore, we investigated its scalability and applicability to applications of different structures, sizes, and criticality levels, using synthetic workflows that we generated for this purpose. In contrast to the qualitative comparison with state-of-the-art approaches presented in Section 2, a meaningful quantitative comparative evaluation is not applicable, as existing techniques (whether heuristic or exact) neither consider the specific edge-hub-cloud environment, nor address all objectives and constraints of our framework. Furthermore, adapting exact methods (e.g., [21, 35]) to accommodate all aspects of our framework would result in formulations essentially equivalent to the one proposed in this work, which is among our key contributions, offering limited additional insight. Nevertheless, to further assess and highlight the strengths of our method, we provide a comparative evaluation

Table 2: Main notations.

Notation	Definition
\mathcal{T}	Set of tasks of the considered workflow application.
\mathcal{U}	Set of computational devices in the target system.
Q_i	Subset of computational devices where task i can be allocated ($Q_i \subseteq \mathcal{U}$).
i, j	Tasks of the application ($i, j \in \mathcal{T}$).
k, l, m, n, o	Computational devices in the target system ($k, l, m, n, o \in \mathcal{U}$).
$G = (\mathcal{N}, \mathcal{A})$	Initial task graph (TG) of the application, where \mathcal{N} and \mathcal{A} are the sets of its nodes and arcs, respectively.
$\tilde{G} = (\tilde{\mathcal{N}}, \tilde{\mathcal{A}})$	Intermediate edge-hub-cloud graph (EG), where $\tilde{\mathcal{N}}$ and $\tilde{\mathcal{A}}$ are the sets of its composite nodes and arcs, respectively.
$\hat{G} = (\hat{\mathcal{N}}, \hat{\mathcal{A}})$	Final reliability-aware edge-hub-cloud graph (REG), where $\hat{\mathcal{N}}$ and $\hat{\mathcal{A}}$ are the sets of its composite nodes and arcs, respectively.
\tilde{N}_i	Composite node in \tilde{G} ($\tilde{N}_i \in \tilde{\mathcal{N}}$), consisting of sets of nodes N_{ik} .
\hat{N}_{ik}	Set in \hat{N}_i , consisting of candidate nodes N_{ik} .
N_{ik}^z	Candidate node N_{ik} , N_{ikl} , or N_{iklm} in \hat{N}_{ik} , corresponding to the possible allocation of primary task i on device k , and its replicas (if applicable) on devices l and m .
r_{in}^z	Primary task i (if $z = 1$) or one of its replicas (if $z \in \{2, 3\}$), allocated on device n , corresponding to candidate node N_{ik}^z .
$\tilde{A}_{i \rightarrow j}$	Composite arc in \tilde{G} ($\tilde{A}_{i \rightarrow j} \in \tilde{\mathcal{A}}$), consisting of individual arcs $A_{ik \rightarrow jl}$.
$A_{ik \rightarrow jl}$	Arc in $\tilde{A}_{i \rightarrow j}$, corresponding to the communication between the sets of nodes \tilde{N}_{ik} and \tilde{N}_{jl} .
ϵ_{ik}	Execution mode of task i when allocated on device k .
ν_i	Number of child tasks of task i .
M_i	Main memory required by task i .
S_i	Storage required by task i .
D_i	Size of output data generated by task i .
L_{in}	Execution time of task i on device n .
P_{in}	Power required to execute task i on device n .
E_{in}	Energy required to execute task i on device n .
V_{in}	Vulnerability factor of task i on device n .
R_{in}	Reliability of task i on device n .
L_{ik}	Total latency of candidate node N_{ik} .
$E_{in}^{z, ik}$	Total energy required by device n to execute primary task or replica r_{in}^z of candidate node N_{ik} .
V_{ik}	Total vulnerability factor of candidate node N_{ik} .
R_{ik}	Total reliability of candidate node N_{ik} .
$\zeta_{ik \rightarrow jl}^o$	Binary parameter indicating whether arc $A_{ik \rightarrow jl}$ involves indirect communication between devices k and l through device o .
$CL_{ik \rightarrow jl}$	Communication latency of arc $A_{ik \rightarrow jl}$.
$CE_{ik \rightarrow jl}$	Communication energy consumption of arc $A_{ik \rightarrow jl}$.
σ_{kl}	Bandwidth of the communication channel between devices k and l .
τ_{kl}, ρ_{kl}	Energy required to transmit and receive, respectively, a unit of data between devices k and l .
Λ	Criticality level of the application.
VT_{DE}, VT_{TE}	Vulnerability threshold of the application for dual and triple task execution, respectively.
$\beta_k^{DE}, \beta_k^{TE}$	Time required to perform the comparison and voting, respectively, on device k .
$\gamma_k^{DE}, \gamma_k^{TE}$	Power required to perform the comparison and voting, respectively, on device k .
$\delta_k^{DE}, \delta_k^{TE}$	Energy required to perform the comparison and voting, respectively, on device k .
x_{ik}	Binary decision variable corresponding to candidate node $N_{ik} \in \hat{G}$.
$x_{ik \rightarrow jl}$	Binary decision variable corresponding to arc $A_{ik \rightarrow jl} \in \hat{G}$.
$x_{in}^{z, ik}$	Auxiliary binary decision variable corresponding to primary task or replica $r_{in}^z \in N_{ik}$.
x_{ik}	Auxiliary binary decision variable corresponding to set $\hat{N}_{ik} \in \hat{G}$.
w_{rel}, w_{lat}	Weights reflecting the relative importance of overall reliability and latency, respectively, in multi-objective function g .
$M_n^{bgt}, S_n^{bgt}, E_n^{bgt}$	Memory, storage, and energy budgets, respectively, of device n .

against three baseline task allocation strategies in the real-world workflow case.

4.1. Experimental setup

While the proposed framework can accommodate multiple devices per layer in the edge-hub-cloud continuum, our evaluation focused on applications for which a single edge device, a single hub device, and a single cloud server suffice, as discussed in Section 1. In our experiments, the edge device (e), the hub device (h), and the cloud server (c) were based on typical real-world counterparts, as shown in Table 3. Parameters M_n^{bgt} , S_n^{bgt} , and E_n^{bgt} were based on the resource limitations of each device n , whereas $\beta_n^{DE}, \beta_n^{TE}, \gamma_n^{DE}, \gamma_n^{TE}, P_n^{idle}$, and P_n^{max} were empirically determined using the profiling and power monitoring tools mentioned in Section 4.2.1. The communication channels and their respective parameters (σ_{kl} , τ_{kl} , and ρ_{kl}), which were based on real-world measurements [4, 45–47], are included in Table 4. As we employ an offline approach, all model parameters were treated as fixed inputs during optimization, instantiated with conservative values derived from real-world measurements and profiling to ensure feasibility under adverse operating conditions. In line with the critical nature of the tar-

geted use cases, the edge, hub, and cloud devices were reserved exclusively for the considered workflow application, ensuring that their computational resources were dedicated to its execution. It is noted that the framework can be re-executed with different parameter sets to enable design-time evaluation of alternative network or workload conditions. For the weights w_{rel} and w_{lat} of the considered objectives we used values in the interval $[0, 1]$. We increased/decreased each weight by 0.05 increments/decrements to investigate a wide range of cases. We considered applications with a low ($\Lambda = 1$), moderate ($\Lambda = 2$), and high ($\Lambda = \Lambda_{max} = 3$) criticality level. For each Λ , we experimented with the vulnerability thresholds VT_{DE} and VT_{TE} shown in Table 5, and the adjustment coefficients $\kappa = 0.06$ and $\lambda = 3$. We selected the particular values so that in each case the vulnerability thresholds would be realistic and aligned with prior studies [16, 42, 43], but still challenging. We implemented the proposed framework, including the resulting BILP formulation, in C++. The resulting BILP model was solved using Gurobi Optimizer 10 [44] with default parameter settings, on a server equipped with an Intel Xeon Gold 6240 processor @ 2.6 GHz and 400 GiB of RAM. No parameter tuning strategies

Table 3: Computational devices & task execution mode percentages per device for $\Lambda = 3$.

Device n	e/h/c	Processor	β_n^{DE} (μs)	β_n^{TE} (μs)	γ_n^{DE} (W)	γ_n^{TE} (W)	M_n^{bgt} (GiB)	S_n^{bgt} (GiB)	E_n^{bgt} (Wh)	P_n^{idle} (W)	P_n^{max} (W)	Exec. Mode % ($\Lambda = 3$)		
												SE	DE	TE
Raspberry Pi 3 Model B	e	Broadcom Cortex A53 @ 1.4 GHz	1.00	1.50	1.20	1.21	1	16	129.96 ^a	1.2	4.5	5%	20%	75%
Mi Notebook Pro	h	Intel i5 8250U @ 1.6 GHz	0.02	0.03	8.02	8.03	8	512	60.00 ^b	8.0	44.0	20%	35%	45%
HPE ProLiant DL580 Gen10	c	Intel Xeon Gold 6240 @ 2.6 GHz	0.01	0.02	75.23	75.26	400	10 240	-	75.0	900.0	35%	50%	15%

^aBattery capacity of DJI Matrice 100 UAV where device e is attached.

^bBattery capacity of device h.

were required, as our framework uses fixed model parameters and the solver was run with default settings.

4.2. Real-world workflow application

4.2.1. Overview

The considered real-world application is used for the autonomous UAV-based aerial inspection of power transmission towers and lines [3]. Its tasks are described in Table 6. Its TG G is depicted in Fig. 2, where tasks are shown in different colors based on their grouping in Table 6. Task N_1 is responsible for capturing an image through a camera mounted on the UAV. Tasks N_2 – N_5 perform the initial processing of the captured image, while tasks N_6 – N_9 apply a Hough transform-based line detector to identify power transmission lines for navigation purposes and to detect issues such as vegetation encroachment. On the other hand, tasks N_{10} – N_{14} utilize a convolutional neural network-based detector to identify power transmission towers and to detect problems such as faulty insulators, while task N_{15} is responsible for displaying the inspection results. Based on their specific functions, tasks N_1 and N_{15} can only be allocated on devices e and h, respectively. In contrast, tasks N_2 – N_{14} can be allocated on any device (e, h, or c).

As the examined application concerns the inspection of a critical infrastructure, we considered that its criticality level is $\Lambda = \Lambda_{\text{max}} = 3$. For each node $N_{ik} \in \dot{G}$ we calculated ϵ_{ik} and V_{ik} so that, using (10) and the vulnerability thresholds for $\Lambda = 3$ in Table 5, the percentage of tasks that required SE, DE, and TE on each device was the one shown in Table 3. We selected the particular percentages based on the criticality level of the application, and considering that device e is less reliable than device h, which in turn is less reliable than device c. We calculated M_i , S_i , D_i , L_{ik} , and P_{ik} by profiling the execution of task i on device k , using PowerTOP, perf, Sysprof, and a digital power monitoring tool, with measurements selected to reflect conservative operating conditions [48, 49]. E_{ik} and R_{ik} were determined using (5) and (9), respectively, whereas v_i was derived from the structure of G . For each arc $A_{ik \rightarrow jl} \in \dot{G}$, we determined $\zeta_{ik \rightarrow jl}^o$ based on the structure of \dot{G} , and we calculated $CL_{ik \rightarrow jl}$ and $CE_{ik \rightarrow jl}$ using (4) and (6), respectively. The primary task and its replicas $r_{in}^z \in N_{ik}$ in \dot{G} inherited their parameters from the respective nodes $N_{in} \in \dot{G}$. For each candidate node $N_{ik} \in \dot{G}$, we calculated the aggregate parameters L_{ik} , $E_{in}^{z, ik}$, V_{ik} , and R_{ik} , using (21)–(24). Each arc $A_{ik \rightarrow jl} \in \dot{G}$ had the same parameters as $A_{ik \rightarrow jl} \in \dot{G}$. The number of nodes and arcs in G , \dot{G} , and \ddot{G} for the real-world workflow are shown in Table 7.

Table 4: Communication channels.

Comm. Channel Between $k \rightarrow l$	σ_{kl} (Mbit/s)	τ_{kl} ($\mu\text{J/bit}$)	ρ_{kl} ($\mu\text{J/bit}$)
e \rightarrow h	11.0	1.0	0.70
h \rightarrow e	8.5	1.0	0.70
h \rightarrow c	12.5	2.5	1.25
c \rightarrow h	20.0	2.5	1.25

Table 6: Real-world workflow tasks.

Task Description	
Image Acquisition	
N_1	Capture image
Image Preprocessing	
N_2	Grayscale processing
N_3	Gamma correction
N_4	Range filter
N_5	Edge detection
Detection of Power Transmission Lines	
N_6	Map edge points to Hough space
N_7	Yield infinite lines
N_8	Convert infinite lines to finite lines
N_9	Reject non-parallel finite lines
Detection of Power Transmission Towers	
N_{10}	Attention mechanism
N_{11}	Image segmentation
N_{12}	Convolutional neural network inference
N_{13}	Acquire and post-process predictions
N_{14}	Draw detection boxes
Display Results	
N_{15}	Visualize inspection findings

Table 5: Vulnerability thresholds.

Λ	VT_{DE}	VT_{TE}
1	0.06	0.18
2	0.03	0.09
3	0.02	0.06

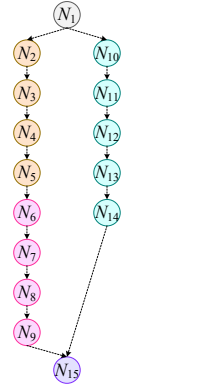


Figure 2: Real-world workflow TG.

Table 7: Node/Arc counts for real-world workflow.

Graph	#Nodes	#Arcs
TG G	15	15
EG \dot{G}	41	111
REG \ddot{G}	153	111

4.2.2. Experimental results

Fig. 3 shows the evaluation results for the real-world application, regarding the normalized overall reliability and latency, with respect to the utilized weights, w_{rel} and w_{lat} . To facilitate the interpretation of the results, the negated normalized latency f''_{lat} is reported as positive (i.e., as if latency were minimized in the combined objective). The allocation of the tasks (primary and replicas) on each device (e, h, and c) is also presented in percentage form for each weight pair. When the objective was set to maximize overall reliability (i.e., $w_{\text{rel}} = 1$), our approach yielded the worst performance in terms of latency. However, although a higher percentage of tasks was expected on device c due to its higher reliability, the tasks were distributed across the three devices, with 26% on device e, 29% on h, and 45% on

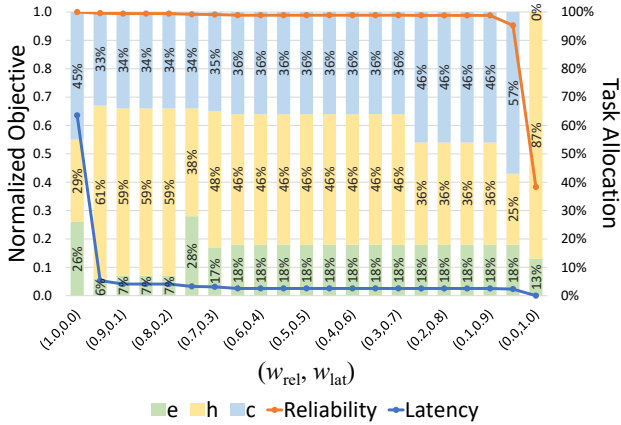


Figure 3: Normalized overall reliability and latency, and percentage of allocated tasks (primary and replicas) per device, with respect to w_{rel} and w_{lat} , for the real-world workflow.

c. On the other hand, when the objective was to minimize the overall latency (i.e., $w_{lat} = 1$), our method provided the minimum reliability. In this case, the tasks were allocated only on devices e and h, with 13% on e and 87% on h. No tasks were allocated on device c, due to the higher communication latency involved.

When we took into account both objectives (i.e., $0 < w_{rel}, w_{lat} < 1$), the majority of tasks were allocated on devices h and c, which generally provided higher reliability and computational capacity, compared to device e. It can also be observed that the overall reliability deteriorated less compared to the overall latency, as we decreased their corresponding weights (and thus their relative importance in the combined objective). When we considered both objectives as equally important (i.e., $w_{rel} = w_{lat} = 0.5$), near-optimal results were achieved for both reliability and latency, as their normalized values (0.99 and 0.02, respectively) were close to the optimal ones (1 and 0, respectively).

As some allocation cases in Fig. 3 were not intuitive (e.g., for $w_{rel} = 1$), a more detailed analysis is presented in Figs. 4 and 5. This analysis aims to provide deeper insights into how our approach allocated the primary tasks and their replicas across the three devices, as well as the utilized task replication technique in each case. Specifically, Fig. 4 illustrates the number of tasks (primary and replicas) per device, with respect to w_{rel} and w_{lat} . Fig. 5 depicts the number of replicas per device in relation to the allocation of their primary counterparts, for each weight pair. It is revealed that when $w_{rel} = 1$, no primary tasks were allocated on device c, even though it provided the highest reliability. In contrast, all of the primary tasks were allocated on devices e and h. However, their replicas (the majority of which were due to TE) were allocated on device c. Evidently, this provided the highest total reliability for the tasks. On the other hand, as we increased the relative importance of latency, the majority of replicas (which were due to TE) were allocated on device h, where their primary tasks were also allocated, as this provided lower latency. This trend was more prominent in the case where $w_{lat} = 1$.

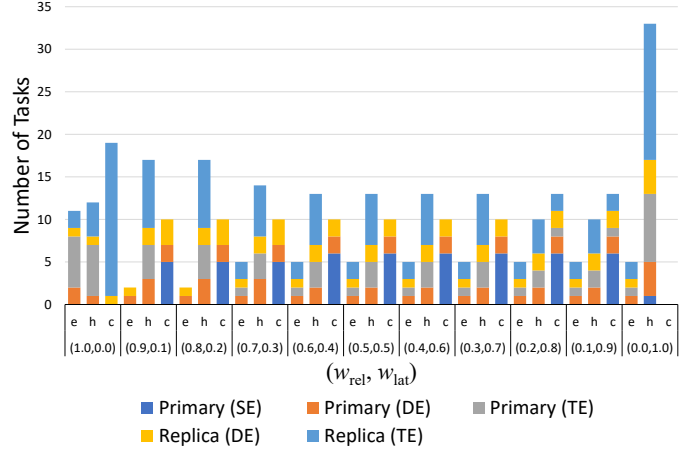


Figure 4: Number of tasks (primary and replicas) per device, with respect to w_{rel} and w_{lat} , for the real-world workflow.

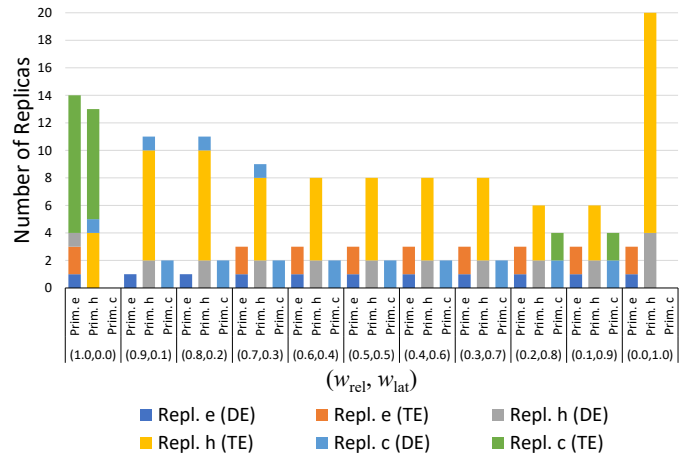


Figure 5: Number of replicas per device, with respect to the allocation of their primary tasks, for w_{rel} and w_{lat} , in the case of the real-world workflow.

Comparison with baseline strategies. To compare the performance of our approach against more restrictive task allocation scenarios, we evaluated it against three baseline strategies where all tasks (primary and replicas) were allocated on device e, h, or c (except for tasks N_1 and N_{15} , which required fixed allocation on devices e and h, respectively). The comparative results regarding the normalized overall reliability and latency, with respect to w_{rel} and w_{lat} , are illustrated in Figs. 6 and 7, respectively. Each baseline strategy is indicated by the device it concerns (e, h, or c). It can be observed that with regard to reliability, the proposed approach outperformed the baseline strategies across all examined weights (except for $w_{rel} = 0$), with an average absolute increase in normalized reliability of 0.36 (on a scale from 0 to 1). In actual (non-normalized) values, the average reliability improvement was 84.19%. For $w_{rel} = 0$, only latency was optimized, resulting in a significant decrease in the reliability yielded by our method. On the other hand, with respect to latency, the proposed approach outperformed the baseline strategies for $w_{lat} = 1$, with an average absolute decrease in normalized latency of 0.05 (on a scale from 0 to 1). In actual (non-normalized) values, the average latency reduction was

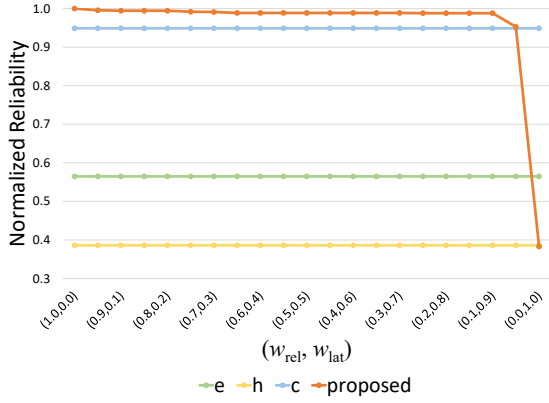


Figure 6: Comparison of proposed approach with baseline strategies (each corresponding to a specific device: e, h, or c) with respect to normalized overall reliability for the real-world workflow, under varying weights w_{rel} and w_{lat} .

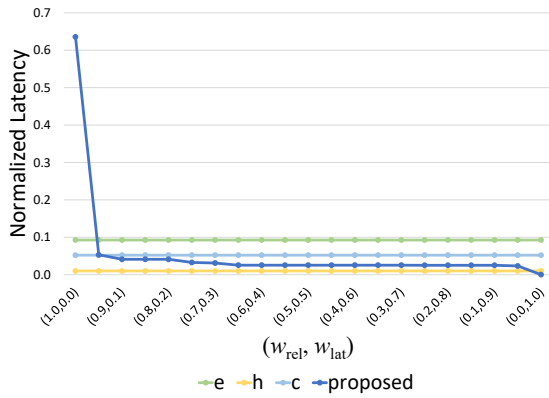


Figure 7: Comparison of proposed approach with baseline strategies (each corresponding to a specific device: e, h, or c) with respect to normalized overall latency for the real-world workflow, under varying weights w_{rel} and w_{lat} .

49.81%. For $0 < w_{lat} < 1$, our method allocated the majority of tasks (primary and replicas) on device h, achieving similar performance to baseline strategy h, which yielded the lowest latency among the three baselines. For $w_{lat} = 0$, the latency provided by the proposed approach increased significantly, as only reliability was optimized in this case. Overall, considering both reliability and latency, the results demonstrate that our method attained an optimized balance between the two objectives, compared to the baseline strategies.

Practical applicability. The evaluation results regarding the real-world application show that the proposed approach highly depended on the relative importance of the two objectives. As reported by the Gurobi solver, our framework required 1653 variables, 1538 constraints, and an average time of 0.04 seconds to return an optimal solution in each case of the examined reliability and latency weights. Consequently, considering the short execution time of the solver, as well as the fact that the experimental results were not always intuitive nor straightforward, our method can facilitate design space exploration with respect to the desired trade-off between reliability and latency.

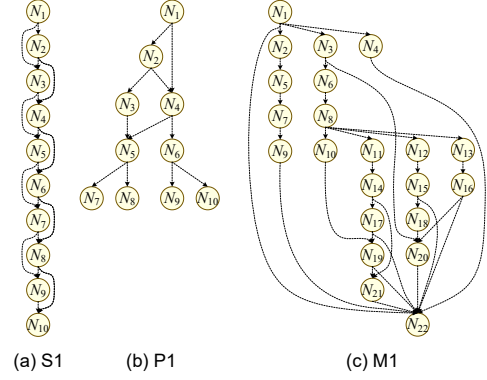


Figure 8: Sample TGs of synthetic workflows with 10 tasks of (a) serial, (b) parallel, and (c) mixed structure. Larger workflows with 100 and 1000 tasks were also generated and examined in our evaluation, as shown in Table 8.

4.3. Synthetic workflow applications

4.3.1. Overview

We generated synthetic workflows using the random TG generator in [50]. The datasets of our synthetically generated workflows are publicly available¹. To examine representative workflow structures and evaluate the broad applicability and scalability of our framework, we generated TGs with serial (S), parallel (P), and mixed (M) structure types (with M being a combination of S and P), comprising 10, 100, and 1000 tasks. The input for the generation of each TG is shown in Table 8. Fig. 8 shows sample TGs generated for each structure type (S1, P1, and M1 in Table 8). Due to the nature of the targeted applications, for each TG we considered that a percentage of randomly selected tasks required fixed allocation on devices e and h, as shown in Table 8. Moreover, we considered three criticality levels, $\Lambda \in \{1, 2, 3\}$, to investigate TGs with low, moderate, and high criticality, respectively.

In the case where the criticality level of a TG G was $\Lambda = 3$, we calculated ϵ_{ik} and V_{ik} in \dot{G} the same way as in the real-world application (Section 4.2.1). In the cases where $\Lambda = 1$ and $\Lambda = 2$, we retained the same V_{ik} as in the case of $\Lambda = 3$. However, we adjusted ϵ_{ik} based on (10) and the corresponding vulnerability thresholds in Table 5. To assign random, yet realistic, values to the rest of the node and arc parameters in \dot{G} , we first ran a number of relevant benchmarks [51, 52] on each device, as shown in Table 9. For the benchmark scores reported in points (pts), higher values indicate better performance (in terms of latency), whereas for those reported in seconds (s), higher values indicate worse performance. We ranked the devices according to their benchmark score, from the slowest (rank 1) to the fastest (rank 3). For each benchmark, we calculated the performance ratio θ_k of each device k . Specifically, for the benchmark scores in points, we calculated θ_k as the ratio of the score of device k to the score of the previous device in the ranking, and for the scores in seconds, as the ratio of the score of the previous device to the score of device k .

Subsequently, we calculated the computational latency L_{ik} for each node $N_{ik} \in \dot{G}$, by first assigning a random value to

¹<https://doi.org/10.5281/zenodo.10357101>

Table 8: Synthetic workflow TGs with their corresponding EGs & REGs per Λ .

TGFF Generator Input			Generated TG		Intermediate EG			Final REG						
SN	#Nodes	In/Out Degree	#Nodes/ Arcs	Fixed Alloc. % (e/h)	#Nodes/ Arcs	#Candidate Nodes/Arcs			#Variables/Constraints			Avg. Execution Time (s)		
						$\Lambda = 1$	$\Lambda = 2$	$\Lambda = 3$	$\Lambda = 1$	$\Lambda = 2$	$\Lambda = 3$	$\Lambda = 1$	$\Lambda = 2$	$\Lambda = 3$
S1	10	2/2	10/17	4/2	30/153	61/153	94/153	94/153	659/626	1542/1476	1542/1476	0.06	0.10	0.10
S2	100	2/2	100/197	4/3	286/1605	924/1605	1091/1605	1145/1605	17498/16782	24409/23526	26827/25890	1.43	2.16	2.10
S3	1000	2/2	1000/1997	5/3	2840/16089	8775/16089	10563/16089	11181/16089	162142/155375	232841/224286	260637/251464	26.78	41.19	50.94
P1	10	2/2	10/11	4/2	28/93	87/93	118/93	123/93	871/809	1552/1459	1794/1696	0.03	0.05	0.06
P2	100	2/3	100/129	4/2	288/1077	860/1077	1039/1077	1103/1077	9925/9249	14580/13725	16664/15745	0.62	0.76	0.90
P3	1000	2/3	999/1232	5/2	2857/10078	8630/10078	10486/10078	11122/10078	99665/92769	144674/135922	162657/153269	15.23	23.46	26.41
M1	10	9/4	22/33	4/1	64/261	184/261	218/261	231/261	2284/2152	3204/3038	3559/3380	0.08	0.12	0.14
M2	100	10/3	109/141	1/3	319/1210	927/1210	1149/1210	1214/1210	11079/10378	17020/16097	18814/17826	0.40	0.72	0.75
M3	1000	12/4	1000/1224	5/2	2864/10055	8572/10055	10411/10055	11046/10055	99339/92775	144911/136508	162719/153681	6.50	10.97	13.68

Table 9: Performance ranking of computational devices.

e/h/c	Device					
	e		h		c	
	Score	Score	θ_h	Score	θ_c	
Benchmark	Raspberry Pi 3 Model B	Mi Notebook Pro		HPE ProLiant DL580 Gen10		
Geekbench 5	398.00 pts	3612.00 pts	9.08	33323.00 pts	9.23	
NumPy	10.63 pts	284.68 pts	26.78	405.71 pts	1.43	
TensorFlow	12648.38 s	169.70 s	74.53	59.82 s	2.84	
Scikit-Learn	1373.54 s	10.11 s	135.86	7.64 s	1.32	
R Benchmark	3.80 s	0.50 s	7.60	0.26 s	1.92	
Rank	1	2		3		

L_{ie} , selected from those measured on device e in the case of the real-world application. We then set L_{ih} and L_{ic} as $L_{ih} = L_{ie}/\theta_h$ and $L_{ic} = L_{ih}/\theta_c$, respectively, where θ_h and θ_c were randomly selected from the respective values in Table 9. Similarly, to determine the power consumption P_{ik} , we first assigned a value to P_{ie} , randomly selected from those measured on device e for the real-world workflow. We then calculated P_{ih} and P_{ic} as $P_{ih} = P_{ie}\theta_h$ and $P_{ic} = P_{ih}\theta_c$, respectively. If the derived P_{ik} was not in the interval $(P_k^{\text{idle}}, P_k^{\text{max}}]$, we adjusted it accordingly. Specifically, if $P_{ik} \leq P_k^{\text{idle}}$, we adjusted it to $P_k^{\text{idle}}(1+\omega)$, whereas if $P_{ik} > P_k^{\text{max}}$, we adjusted it to $P_k^{\text{max}}(1-\omega)$. We randomly selected the adjustment factor ω in $[0.1\%, 0.5\%]$, so that the adjusted value of P_{ik} did not deviate significantly from its initially calculated value.

Furthermore, we randomly selected M_i , S_i , and D_i from the respective values measured in the case of the real-world application. We calculated the rest of the node and arc parameters in \tilde{G} , and subsequently the parameters in \check{G} , as described in Section 4.2.1. The number of nodes and arcs in each synthetic TG, as well as in the corresponding EG and REG (for each criticality level), are shown in Table 8.

4.3.2. Experimental results

The results regarding the normalized overall reliability and latency, with respect to w_{rel} and w_{lat} , for synthetic workflows with criticality level $\Lambda \in \{1, 2, 3\}$ (each evaluated using TGs of serial, parallel, and mixed structure, and with 10, 100, and 1000 tasks), are illustrated in Figs. 9, 10, and 11, respectively. The results also show the percentage of tasks (primary and replicas) that were allocated on devices e, h, and c, in each case. In general, the observations made for the real-world workflow also hold for the synthetic workflows. S1 and P1 are notable exceptions, since as we increased w_{lat} from 0 to 1, more tasks were allocated on device c, instead of device h, in contrast to the other TGs. This occurred, as S1 and P1 had a smaller number

of tasks compared to other TGs, as shown in Table 8. Consequently, for S1 and P1 the calculated percentage of tasks requiring fixed allocation on devices e and h was 0.4, and thus rounded to 0. Therefore, as tasks could be allocated on any device, they were all allocated on device c, which provided the lowest computational latency.

For each of the examined workflow structures, it can be observed that the difference in the results was more prominent between cases with 10 and 100 tasks than between cases with 100 and 1000 tasks. This was due to the fact that TGs with 10 tasks led to significantly different task allocations, compared to those with 100 and 1000 tasks. Moreover, as in the case of the real-world workflow, it can be observed that the overall latency deteriorated more compared to reliability, as we reduced their weights. Thus, the overall latency was more sensitive to the changes in its relative importance, compared to reliability.

Sensitivity to criticality level. For $\Lambda \in \{2, 3\}$, the deterioration in reliability and latency started to occur when their respective weights (and thus their relative importance) were closer to zero. In contrast, for $\Lambda = 1$, the deterioration started to occur at larger weights. The reason was that higher criticality levels resulted in a greater number of task replicas, due to the lower vulnerability thresholds, and thus the overall reliability was improved. In addition, the greater number of replicas also benefited the latency objective for larger w_{lat} , as it forced more primary tasks to be allocated along with their replicas on devices h and c, which provided lower computational latency. Hence, our framework adapted predictably to different levels of application criticality.

Scalability analysis. Table 8 shows the BILP problem size (number of variables and constraints) and the average execution time required to obtain a solution, as reported by the Gurobi solver, for each examined TG. For all TG structures (serial, parallel, and mixed), the solver execution time increased with workflow size. On average, serial TGs required the longest solver runtimes (0.06–50.94 seconds), followed by parallel TGs (0.03–26.41 seconds), while mixed TGs generally required the shortest runtimes (0.08–13.68 seconds). The shorter execution times for mixed TGs were due to their balanced structure, which avoided the long dependency chains of serial TGs and the excessive parallelism of parallel TGs that made finding the optimal task allocation more challenging in those cases. Furthermore, as the criticality level Λ increased, the number of replicas grew, increasing the problem size and thus the solver runtime.

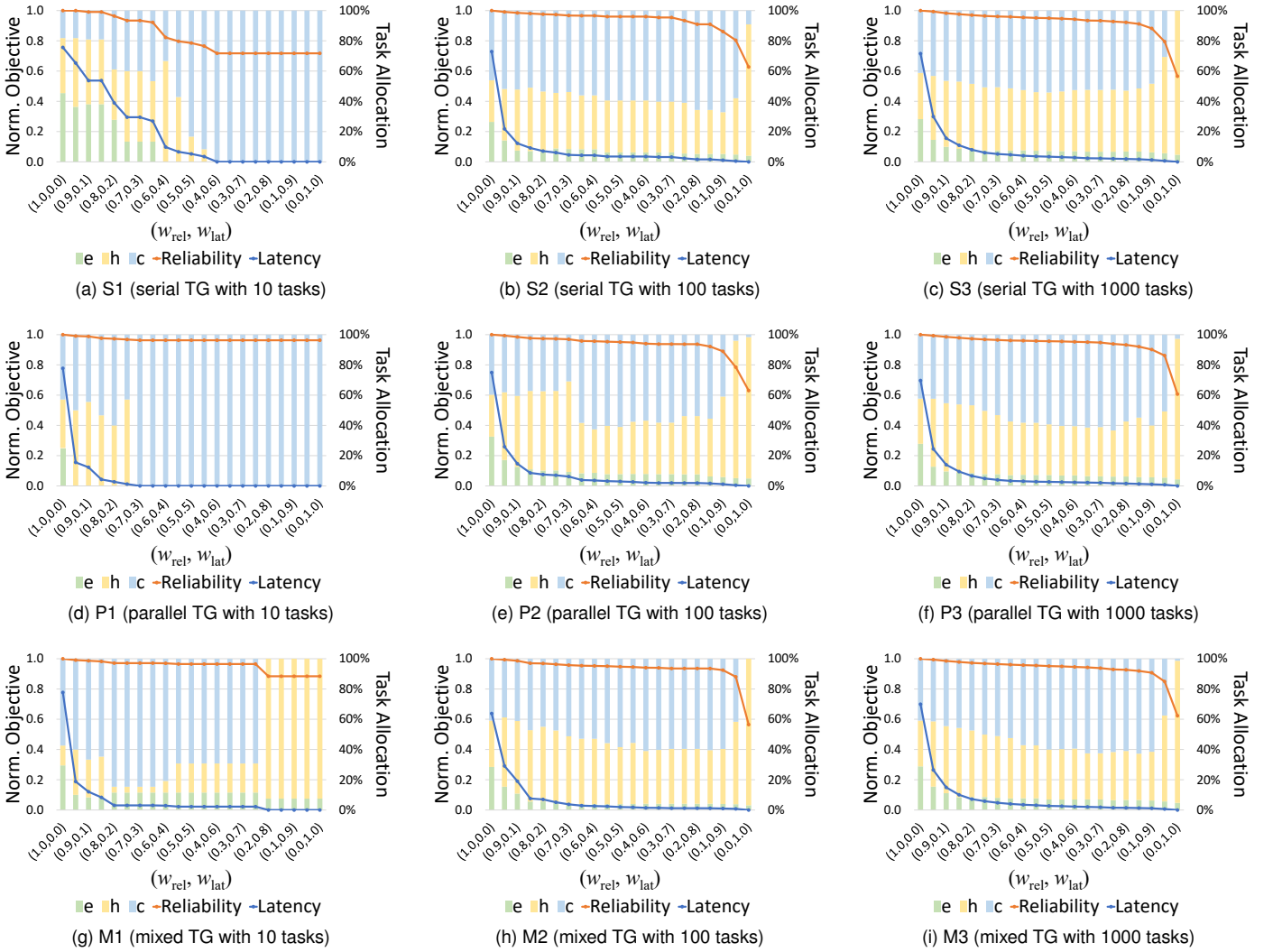


Figure 9: Normalized overall reliability and latency, and percentage of allocated tasks (primary and replicas) per device, with respect to w_{rel} and w_{lat} , for synthetic workflows with $\lambda = 1$.

However, even for TGs with 1000 tasks and high criticality, runtimes remained short and practical for all workflow structures.

Overall, the experimental results demonstrate the scalability and applicability of our approach to workflows of different structures (serial, parallel, and mixed), sizes (10, 100, and 1000 tasks), and criticality levels (low, moderate, and high). The framework consistently provided optimal solutions for the specified trade-offs between reliability and latency in a short time frame, ranging on average from 0.03 to 50.94 seconds. Given that this is an exact, design-time (i.e., offline) method, and considering the NP-hard nature of the problem [13], the solver execution times are both reasonable and practical.

5. Conclusions and future work

We proposed an exact, reliability- and latency-driven multi-objective optimization framework to allocate the tasks of a workflow application in the edge-hub-cloud continuum. We examined a streamlined yet challenging architecture, comprising

an edge device, a hub device, and a cloud server. Our approach utilizes a comprehensive BILP formulation to jointly optimize the overall reliability and latency of the application, while considering constraints often overlooked in related studies, such as the limited memory, storage, and energy capacities of the devices, the reliability requirements of the tasks, as well as the computational and communication latency and energy required for the execution of each task. The proposed formulation is facilitated by a two-step task graph transformation technique. It takes into account the defined trade-off between the reliability and latency goals, as well as the criticality level of the application, while employing widely used time redundancy methods.

We evaluated our framework using a real-world workflow application, as well as representative synthetic workflows that we generated for this purpose. Through extensive experimentation, we demonstrated the effectiveness, scalability, and applicability of our approach to workflows of different structures, sizes, and criticality levels. In the real-world workflow, the proposed method achieved average improvements of 84.19%

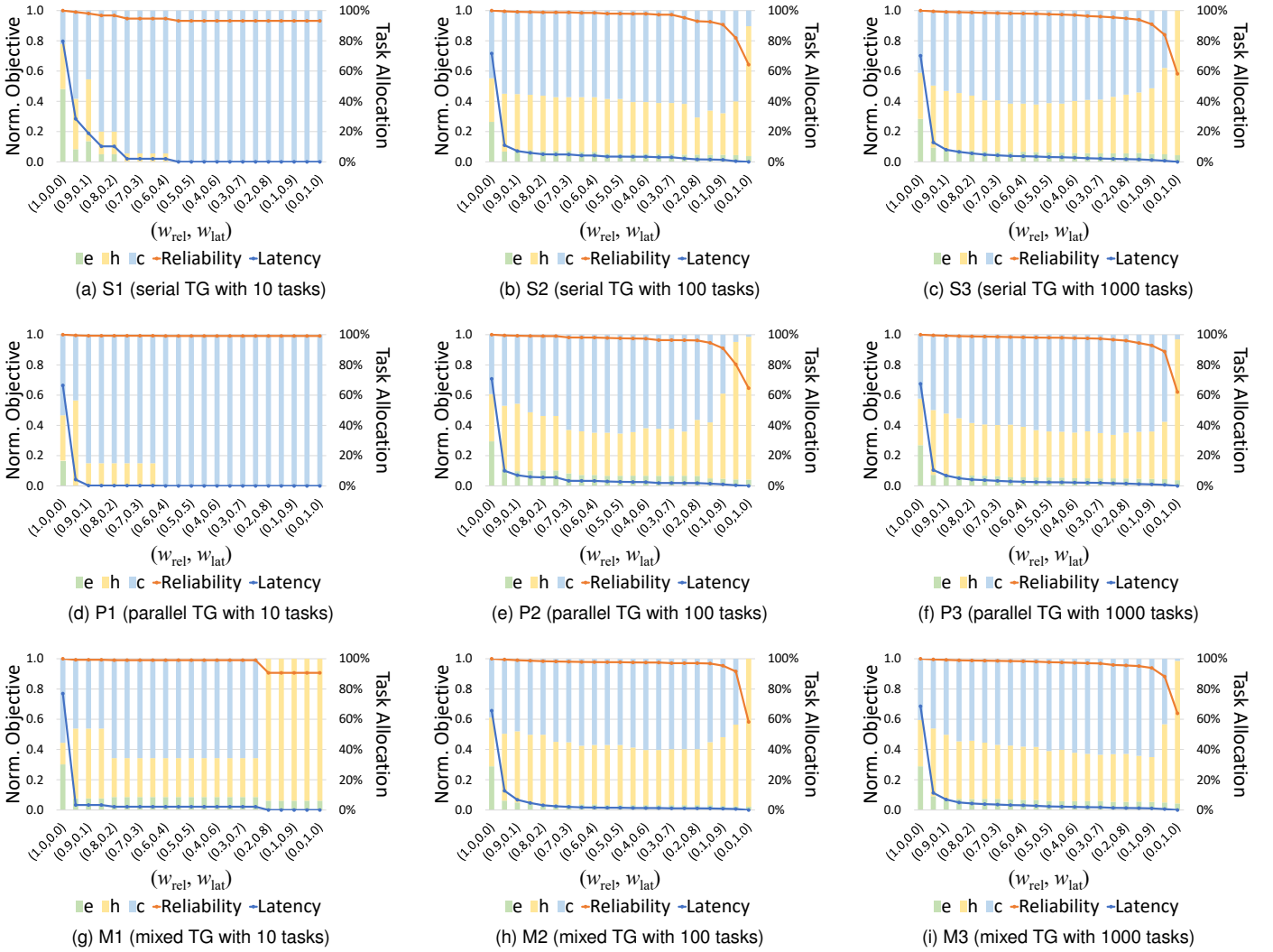


Figure 10: Normalized overall reliability and latency, and percentage of allocated tasks (primary and replicas) per device, with respect to w_{rel} and w_{lat} , for synthetic workflows with $\Lambda = 2$.

in reliability and 49.81% in latency over baseline strategies, across relevant objective trade-offs. The average solution time across all examined task graphs ranged from 0.03 to 50.94 seconds. The usefulness of our framework is further highlighted by experimental results that were sometimes non-intuitive, particularly in how tasks were allocated based on the relative importance of each objective. While this work focuses on critical workflow applications where a single edge device suffices for reliable and efficient operation, in future work we plan to evaluate the proposed framework in scenarios requiring multiple edge devices to assess the additional challenges such architectures entail. Furthermore, we aim to incorporate heuristics for dynamic task allocation and explore machine learning techniques to support online allocation decisions through the prediction of reliability and latency trends.

Acknowledgments

This work has been supported by the European Union's Horizon 2020 research and innovation programme under grant agreement No. 739551 (KIOS CoE) and from the Government of the Republic of Cyprus through the Cyprus Deputy Ministry of Research, Innovation and Digital Policy.

References

- [1] X. Liu, Z. Wang, C. Zhang, B. Cao, M. Fridenfalk, A. Kumar Singh, Multiobjective resource allocation for cloud-edge-terminal collaboration, *IEEE Internet Things J.* 12 (11) (2025) 17024–17033. doi:10.1109/JIOT.2025.3539574.
- [2] S. Abdi, M. Ashjaei, S. Mubeen, Deadline-constrained security-aware workflow scheduling in hybrid cloud architecture, *Future Gener. Comput. Syst.* 162 (2025) 107466. doi:10.1016/j.future.2024.07.044.

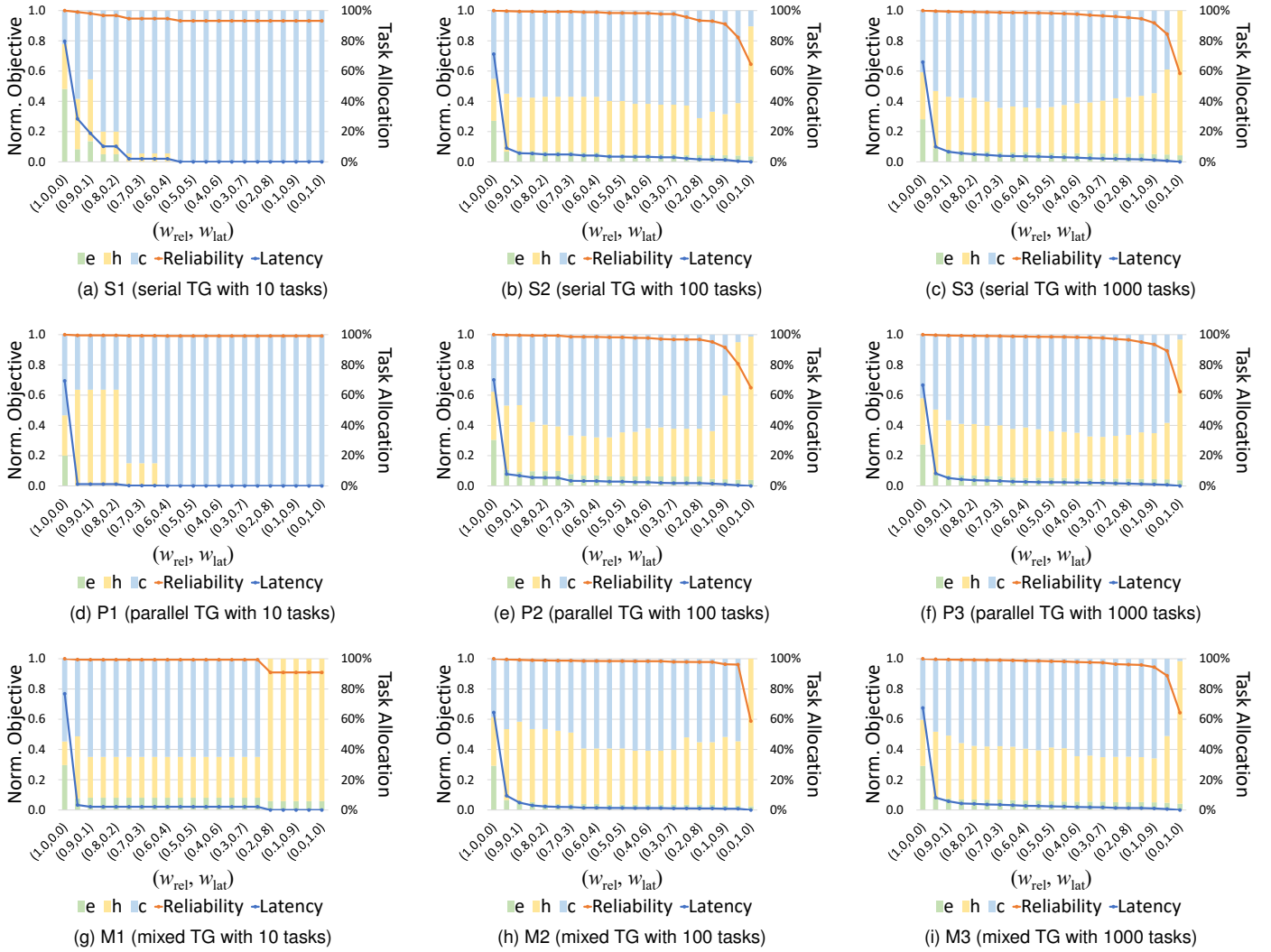


Figure 11: Normalized overall reliability and latency, and percentage of allocated tasks (primary and replicas) per device, with respect to w_{rel} and w_{lat} , for synthetic workflows with $\Lambda = 3$.

- [3] A. Savva, A. Zacharia, R. Makrigrigoris, A. Anastasiou, C. Kyrkou, P. Kolios, C. Panayiotou, T. Theocharides, ICARUS: Automatic autonomous power infrastructure inspection with UAVs, in: Proc. 2021 International Conference on Unmanned Aircraft Systems (ICUAS), 2021, pp. 918–926. doi:10.1109/ICUAS51884.2021.9476742.
- [4] V. Papić, P. Šolić, A. Milan, S. Gotovac, M. Polić, High-resolution image transmission from UAV to ground station for search and rescue missions planning, Appl. Sci. 11 (5) (2021) 2105:1–19. doi:10.3390/app11052105.
- [5] Q. Zheng, Q. Tang, Z. L. Wang, Z. Li, Self-powered cardiovascular electronic devices and systems, Nat. Rev. Cardiol. 18 (1) (2021) 7–21. doi:10.1038/s41569-020-0426-4.
- [6] A. Wang, L. Chen, W. Xu, XPro: A cross-end processing architecture for data analytics in wearables, in: Proc. 44th Annual International Symposium on Computer Architecture (ISCA), 2017, pp. 69–80. doi:10.1145/3079856.3080219.
- [7] S. Agarwal, R. K. Shinde, Smart pacemaker: A review, Cureus 14 (10) (2022) e30027. doi:10.7759/cureus.30027.
- [8] R. Alam, J. Dugan, N. Homdee, N. Gandhi, B. Ghaemmaghami, H. Meda, A. Bankole, M. Anderson, J. Gong, T. Smith-Jackson, J. Lach, BESI: Reliable and heterogeneous sensing and intervention for in-home health applications, in: Proc. 2017 IEEE/ACM International Conference on Connected Health: Applications, Systems and Engineering Technologies (CHASE), 2017, pp. 147–156. doi:10.1109/CHASE.2017.73.
- [9] K. Kolomvatsos, C. Anagnostopoulos, Multi-criteria optimal task allocation at the edge, Future Gener. Comput. Syst. 93 (2019) 358–372. doi:10.1016/j.future.2018.10.051.

- [10] N. Rasouli, C. Klein, E. Elmroth, Resource management for mission-critical applications in edge computing: Systematic review on recent research and open issues, *ACM Comput. Surv.* 58 (3) (2026) 71:1–71:37. doi:10.1145/3762181.
- [11] L. Mo, Q. Zhou, A. Kritikakou, X. Cao, Energy optimized task mapping for reliable and real-time networked systems, *ACM Trans. Sen. Netw.* 19 (4) (2023) 1–26. doi:10.1145/3584985.
- [12] M. Ottavi, S. Pontarelli, D. Gizopoulos, C. Bolchini, M. K. Michael, L. Anghel, M. Tahoori, A. Paschalis, P. Reviriego, O. e. a. Bringmann, Dependable multicore architectures at nanoscale: The view from Europe, *IEEE Des. Test* 32 (2) (2014) 17–28. doi:10.1109/MDAT.2014.2359572.
- [13] E. A. Khalil, S. Ozdemir, S. Tosun, Evolutionary task allocation in Internet of Things-based application domains, *Future Gener. Comput. Syst.* 86 (2018) 121–133. doi:10.1016/j.future.2018.03.033.
- [14] O. Grodzevich, O. Romanko, Normalization and other topics in multi-objective optimization, in: *Proc. First Fields–MITACS Industrial Problems Workshop, 2006*, pp. 89–101.
- [15] A. Kouloumpris, M. K. Michael, T. Theocharides, Reliability-aware task allocation latency optimization in edge computing, in: *Proc. IEEE 25th International Symposium on On-Line Testing and Robust System Design (IOLTS), 2019*, pp. 200–203. doi:10.1109/IOLTS.2019.8854422.
- [16] A. Kouloumpris, T. Theocharides, M. K. Michael, Cost-effective time-redundancy based optimal task allocation for the edge-hub-cloud systems, in: *Proc. 2020 IEEE Computer Society Annual Symposium on VLSI (ISVLSI), 2020*, pp. 368–373. doi:10.1109/ISVLSI49217.2020.00074.
- [17] Z. Fang, H. Yu, G. Fan, Z. Li, J. Zhang, Energy, cost and reliability-aware workflow scheduling on multi-cloud systems: A multi-objective evolutionary approach, *IEEE Trans. Netw. Serv. Manag.* 22 (5) (2025) 4788–4805. doi:10.1109/TNSM.2025.3587108.
- [18] Q. Jiang, X. Xin, T. Zhang, K. Chen, Energy-efficient task scheduling and resource allocation in edge-heterogeneous computing systems using multiobjective optimization, *IEEE Internet Things J.* 12 (17) (2025) 36747–36764. doi:10.1109/JIOT.2025.3584183.
- [19] S. Nastic, T. Pusztai, A. Morichetta, V. C. Pujol, S. Dustdar, D. Vii, Y. Xiong, Polaris scheduler: Edge sensitive and SLO aware workload scheduling in cloud-edge-IoT clusters, in: *Proc. IEEE 14th International Conference on Cloud Computing (CLOUD), 2021*, pp. 206–216. doi:10.1109/CLOUD53861.2021.00034.
- [20] C. Li, J. Li, Y. Gao, J. Song, Z. Wang, Multidimensional resource load-aware task migration in mobile edge computing, *Future Gener. Comput. Syst.* 175 (2026) 108091. doi:10.1016/j.future.2025.108091.
- [21] J. Santos, C. Wang, T. Wauters, F. De Turck, Diktyo: Network-aware scheduling in container-based clouds, *IEEE Trans. Netw. Serv. Manag.* 20 (4) (2023) 4461–4477. doi:10.1109/TNSM.2023.3271415.
- [22] A. Marchese, O. Tomarchio, Application and infrastructure-aware orchestration in the cloud-to-edge continuum, in: *Proc. IEEE 16th International Conference on Cloud Computing (CLOUD), 2023*, pp. 262–271. doi:10.1109/CLOUD60044.2023.00037.
- [23] X. Wang, C. S. Yeo, R. Buyya, J. Su, Optimizing the makespan and reliability for workflow applications with reputation and a look-ahead genetic algorithm, *Future Gener. Comput. Syst.* 27 (8) (2011) 1124–1134. doi:10.1016/j.future.2011.03.008.
- [24] X. Tang, Reliability-aware cost-efficient scientific workflows scheduling strategy on multi-cloud systems, *IEEE Trans. Cloud Comput.* 10 (4) (2022) 2909–2919. doi:10.1109/TCC.2021.3057422.
- [25] S. Khurana, G. Sharma, M. Kumar, N. Goyal, B. Sharma, Reliability based workflow scheduling on cloud computing with deadline constraint, *Wireless Pers. Commun.* 130 (2) (2023) 1417–1434. doi:10.1007/s11277-023-10337-z.
- [26] Y. Asghari-Alaie, M. Hosseini-Shirvani, A. M. Rahmani, A hybrid bi-objective scheduling algorithm for execution of scientific workflows on cloud platforms with execution time and reliability approach, *J. Supercomput.* 79 (2) (2023) 1451–1503. doi:10.1007/s11277-022-04703-0.
- [27] H. Wang, Y. Wang, Maximizing reliability and performance with reliability-driven task scheduling in heterogeneous distributed computing systems, *J. Ambient Intell. Humaniz. Comput.* (2018) 1–11doi:10.1007/s12652-018-0926-9.
- [28] J. Huang, R. Li, X. Jiao, Y. Jiang, W. Chang, Dynamic DAG scheduling on multiprocessor systems: reliability, energy, and makespan, *IEEE Trans. Comput. Aided Des. Integr. Circuits Syst.* 39 (11) (2020) 3336–3347. doi:10.1109/TCAD.2020.3013045.
- [29] A. Taghinezhad-Niar, J. Taheri, Reliability, rental-cost and energy-aware multi-workflow scheduling on multi-cloud systems, *IEEE Trans. Cloud Comput.* 11 (3) (2023) 2681–2692. doi:10.1109/TCC.2022.3223869.
- [30] A. Taghinezhad-Niar, J. Taheri, Security, reliability, cost, and energy-aware scheduling of real-time workflows in compute-continuum environments, *IEEE Trans. Cloud*

- Comput. 12 (3) (2024) 954–965. doi:10.1109/TCC.2024.3426282.
- [31] S. Saeedi, R. Khorsand, S. Ghandi Bidgoli, M. Ramezanzpour, Improved many-objective particle swarm optimization algorithm for scientific workflow scheduling in cloud computing, *Comput. Ind. Eng.* 147 (2020) 106649. doi:10.1016/j.cie.2020.106649.
- [32] J. Peng, K. Li, J. Chen, K. Li, Reliability/performance-aware scheduling for parallel applications with energy constraints on heterogeneous computing systems, *IEEE Trans. Sustain. Comput.* 7 (3) (2022) 681–695. doi:10.1109/TSUSC.2022.3146138.
- [33] V. De Maio, D. Kimovski, Multi-objective scheduling of extreme data scientific workflows in fog, *Future Gener. Comput. Syst.* 106 (2020) 171–184. doi:10.1016/j.future.2019.12.054.
- [34] M. I. Khaleel, Hybrid cloud-fog computing workflow application placement: Joint consideration of reliability and time credibility, *Multimed. Tools Appl.* 82 (2023) 18185–18216. doi:10.1007/s11042-022-13923-8.
- [35] R. Ramezani, A. Ghavidel, Y. Sedaghat, Exact and efficient reliability and performance optimization of synchronous task graphs, *Reliab. Eng. Syst. Saf.* 205 (2021) 107223. doi:10.1016/j.res.2020.107223.
- [36] F. Guisheng, C. Liang, Y. Huiqun, Q. Wei, Multi-objective optimization of container-based microservice scheduling in edge computing, *Comput. Sci. Inf. Syst.* 18 (1) (2021) 23–42. doi:10.2298/CSIS200229041F.
- [37] A. Kouloumpri, G. L. Stavrinides, M. K. Michael, T. Theocharides, An optimization framework for task allocation in the edge/hub/cloud paradigm, *Future Gener. Comput. Syst.* 155 (2024) 354–366. doi:10.1016/j.future.2024.02.005.
- [38] A. Kouloumpri, G. L. Stavrinides, M. K. Michael, T. Theocharides, Optimal multi-constrained workflow scheduling for cyber-physical systems in the edge-cloud continuum, in: *Proc. IEEE Annu. Comput. Softw. Appl. Conf. (COMPSAC)*, 2024, pp. 483–492. doi:10.1109/COMPSAC61105.2024.00072.
- [39] G. L. Stavrinides, H. D. Karatza, An energy-efficient, QoS-aware and cost-effective scheduling approach for real-time workflow applications in cloud computing systems utilizing DVFS and approximate computations, *Future Gener. Comput. Syst.* 96 (2019) 216–226. doi:10.1016/j.future.2019.02.019.
- [40] S. S. Mukherjee, C. Weaver, J. Emer, S. K. Reinhardt, T. Austin, A systematic methodology to compute the architectural vulnerability factors for a high-performance microprocessor, in: *Proc. 36th Annual IEEE/ACM International Symposium on Microarchitecture (MICRO)*, 2003, pp. 29–40. doi:10.1109/MICRO.2003.1253181.
- [41] M. Maniatakos, M. Michael, C. Tirumurti, Y. Makris, Revisiting vulnerability analysis in modern microprocessors, *IEEE Trans. Comput.* 64 (9) (2015) 2664–2674. doi:10.1109/TC.2014.2375232.
- [42] G. Xie, G. Zeng, Y. Chen, Y. Bai, Z. Zhou, R. Li, K. Li, Minimizing redundancy to satisfy reliability requirement for a parallel application on heterogeneous service-oriented systems, *IEEE Trans. Serv. Comput.* 13 (5) (2020) 871–886. doi:10.1109/TSC.2017.2665552.
- [43] N. Kherraf, S. Sharafeddine, C. M. Assi, A. Ghayeb, Latency and reliability-aware workload assignment in IoT networks with mobile edge clouds, *IEEE Trans. Netw. Serv. Manag.* 16 (4) (2019) 1435–1449. doi:10.1109/TNSM.2019.2946467.
- [44] Gurobi Optimization, <https://www.gurobi.com>, Accessed: Apr. 7 (2025).
- [45] J. Huang, F. Qian, A. Gerber, Z. M. Mao, S. Sen, O. Spatscheck, A close examination of performance and power characteristics of 4G LTE networks, in: *Proc. 10th International Conference on Mobile systems, Applications, and Services (MobiSys)*, 2012, pp. 225–238. doi:10.1145/2307636.2307658.
- [46] Y. Shi, R. Enami, J. Wensowitch, J. Camp, UABeam: UAV-based beamforming system analysis with in-field air-to-ground channels, in: *Proc. 15th Annual IEEE International Conference on Sensing, Communication, and Networking (SECON)*, 2018, pp. 1–9. doi:10.1109/SAHCN.2018.8397110.
- [47] 5G Americas, New services & applications with 5G ultra-reliable low latency communications, White paper, 5G Americas (Nov. 2018).
- [48] PowerTOP, <https://github.com/fenrus75/powerTOP>, Accessed: Apr. 7 (2025).
- [49] Sysprof, <https://www.sysprof.com>, Accessed: Apr. 7 (2025).
- [50] R. P. Dick, D. L. Rhodes, W. Wolf, TGFF: Task graphs for free, in: *Proc. Sixth International Workshop on Hardware/Software Codesign (CODES/CASHE)*, 1998, pp. 97–101. doi:10.1109/HSC.1998.666245.
- [51] OpenBenchmarking, <https://openbenchmarking.org>, Accessed: Apr. 7 (2025).
- [52] Geekbench, <https://www.geekbench.com>, Accessed: Apr. 7 (2025).